ADVANCED MATERIALS
www.advmat.de

An Engineered Nanosugar Enables Rapid and Sustained Glucose-Responsive Insulin Delivery in Diabetic Mice

Rong Xu, Sukhvir Kaur Bhangu, Karly C. Sourris, Domitilla Vanni, Marc-Antoine Sani, John A. Karas, Karen Alt, Be'eri Niego, Anukreity Ale, Quinn A. Besford, Brendan Dyett, Joshua Patrick, Irena Carmichael, Jonathan E. Shaw, Frank Caruso, Mark E. Cooper, Christoph E. Hagemeyer, and Francesca Cavalieri**

Glucose-responsive insulin-delivery platforms that are sensitive to dynamic glucose concentration fluctuations and provide both rapid and prolonged insulin release have great potential to control hyperglycemia and avoid hypoglycemia diabetes. Here, biodegradable and charge-switchable phytoglycogen nanoparticles capable of glucose-stimulated insulin release are engineered. The nanoparticles are "nanosugars" bearing glucose-sensitive phenylboronic acid groups and amine moieties that allow effective complexation with insulin (≈95% loading capacity) to form nanocomplexes. A single subcutaneous injection of nanocomplexes shows a rapid and efficient response to a glucose challenge in two distinct diabetic mouse models, resulting in optimal blood glucose levels (below 200 mg dL^{-1}) for up to 13 h. The morphology of the nanocomplexes is found to be key to controlling rapid and extended glucose-regulated insulin delivery in vivo. These studies reveal that the injected nanocomplexes enabled efficient insulin release in the mouse, with optimal bioavailability, pharmacokinetics, and safety profiles. These results highlight a promising strategy for the development of a glucose-responsive insulin delivery system based on a natural and biodegradable nanosugar.

1. Introduction

Diabetes mellitus (type 1 and type 2) is a group of metabolic disorders associated with persistent hyperglycemia (high blood glucose levels) that currently affects more than 463 million people worldwide and an estimated 700 million people by 2045.[1] Frequent subcutaneous (SC) administration of exogenous insulin formulations (rapid, short, intermediate, or long acting)[2] combined with blood glucose level monitoring by finger-prick tests or in-arm continuous blood glucose monitoring sensors remain the main strategy for blood glucose management and treatment of type 1 diabetes as well as some type 2 diabetes. However, SC administration of insulin is often associated with hypoglycemia, which can be life threatening, and leads to glucose fluctuations

R. Xu, K. Alt, B. Niego, A. Ale, J. Patrick, C. E. Hagemeyer
Australian Centre for Blood Diseases
Central Clinical School
Monash University
Melbourne, Victoria 3004, Australia
E-mail: christoph.hagemeyer@monash.edu

S. K. Bhangu, B. Dyett, F. Cavalieri
School of Science
RMIT University
Melbourne, Victoria 3000, Australia
E-mail: francesca.cavalieri@unimelb.edu.au

S. K. Bhangu, D. Vanni, Q. A. Besford,[+] F. Caruso
Department of Chemical Engineering
The University of Melbourne
Parkville, Victoria 3000, Australia

The ORCID identification number(s) for the author(s) of this article can be found under https://doi.org/10.1002/adma.202210392.

[+]Present address: Leibniz-Institut für Polymerforschung e.V.
Hohe Str. 6, 01069 Dresden, Germany

DOI: 10.1002/adma.202210392

K. C. Sourris, M. E. Cooper
Department of Diabetes
Central Clinical School
Monash University
Melbourne, Victoria 3004, Australia

D. Vanni, F. Cavalieri
Dipartimento di Scienze e Tecnologie Chimiche
Universita' di Roma "Tor Vergata"
Via della Ricerca Scientifica 1, Rome 00133, Italy

M.-A. Sani, J. A. Karas
School of Chemistry
The Bio21 Institute
The University of Melbourne
Melbourne, Victoria 3010, Australia

I. Carmichael
Monash Micro Imaging
Monash University
Melbourne, Victoria 3004, Australia

J. E. Shaw
Baker Heart and Diabetes Institute
Melbourne, Victoria 3004, Australia [+]Present address: Leibniz-Institut für Polymer for schung, e.V. Hohe Str. 6, 01069 Dresden, Germany

and other adherence issues.[3] To improve diabetes therapy, a glucose-responsive insulin delivery system that can act as an insulin reservoir, after a single daily SC injection, would be desirable. Such a system will rapidly deploy insulin to counteract spikes in blood glucose levels and ensure a sustained release of insulin to maintain extended normoglycemia. In addition, the ideal insulin delivery system would display sufficient insulin-loading capacity, colloidal stability for storage and administration together with a long shelf life and cost effectiveness. A simple, reproducible, and scalable manufacturing process as well as biodegradability with limited toxicity and immunogenicity are also highly desirable.[4]

To date, formulations that dynamically regulate insulin release in response to blood glucose are not clinically available. Various glucose-responsive materials for insulin delivery have been preclinically investigated for the controlled delivery of insulin in diabetic animal models, including glucose oxidase enzyme (GOx) based hydrogels,[5] GOx loaded nanoparticles (NPs),[6] or concanavalin A (ConA) based microparticles,[7] and phenyl boronic acid (PBA)-based microspheres,[8] complexes,[9] liposomes,[10] microneedles,[11] cells[12] and insulin analogues.[13] Among other glucose-responsive materials that have been investigated, a glucose-responsive, charge-switchable complex based on nonbiodegradable cationic boronated polyacrylamide[14] and water-insoluble micrometer-sized poly-L-lysine (PLL)[15] has been validated, displaying robust glucose-triggered insulin release in diabetic pig and mouse models. However, those systems face long-term biocompatibility issues due to the nonbiodegradable acrylic polymer chains and variability in the insulin release profile that is affected by rapid and uncontrolled aggregation of the PLL–boronate–insulin mixture. Notably, variability in the effect of SC absorption of insulin can give rise to an unpredictable therapeutic response, resulting in inadequate glycemic control or increased risk of hypoglycaemia.[16] Glucose-responsive nanocomplexes (NCs) in the form of a stable colloidal dispersion may potentially enable better control of the insulin release profile. As a possible candidate, glycogen, a natural nanosugar (also referred to as a polysaccharide NP), displays inherent biocompatibility, surface hydrophilicity, and structural flexibility, and can be chemically modified with relative ease.[17]

Here, we present a glucose-responsive NP system based on a nanosugar sourced from sweet corn, also known as phytoglycogen (PG). Charge-switchable PG NPs (hereafter referred to as $PG_{EDA\text{-}FPBA}$ NPs) were synthesized with chemical derivatization with ethylenediamine (EDA) and 4-Carboxy-3-fluorophenylboronic acid (FPBA) to enable effective complexation with insulin forming nanocomplexes (Ins-$PG_{EDA\text{-}FPBA}$ NCs). These NCs demonstrated a rapid and sustained glucose-responsive release of insulin in a therapeutically relevant dose and time scale. Imaging by stochastic optical reconstruction microscopy (STORM) revealed that the morphologies of Ins-$PG_{EDA\text{-}FPBA}$ NCs are pivotal in controlling the rapid and extended glucose-regulated insulin delivery. Direct evidence in spontaneously Akita and streptozotocin (STZ) chemically induced type 1 diabetic mouse models showed that a single SC administration of Ins-$PG_{EDA\text{-}FPBA}$ NCs displayed pronounced glucose-responsiveness in vivo. Finally, the fate and biocompatibility of the Ins-$PG_{EDA\text{-}FPBA}$ NCs were evaluated in these diabetic mouse models.

2. Results and Discussion

2.1. Engineering Charge-Switchable Nanosugars for Glucose-Responsive Insulin Delivery

PG is a highly branched polysaccharide NP derived from sweet corn with a dendrimer-like molecular structure (**Figure 1**a) composed of repeating units of glucose connected by linear α-D-(1-4) glycosidic linkages with α-D-(1-6) branching. The PG NP displayed a multilobular morphology, as shown by the cryo-transmission electron microscopy (cryo-TEM) images (Figure S1a, Supporting Information), a hydrodynamic diameter of ≈80 ± 30 nm (Figure S1b,c, Supporting Information) and a ζ-potential of –5 ± 2 mV (Figure S1d, Supporting Information), as determined by dynamic light scattering (DLS) and electrophoretic mobility measurements, respectively. The PG NPs were endowed with a positive surface charge and glucose sensitive moieties upon chemical derivatization with EDA and FPBA groups in aqueous solvents (Figure S2, Supporting Information) to obtain PG_{EDA} NPs and $PG_{EDA\text{-}FPBA}$ NPs respectively. Briefly, in the PG chains there are two hydroxyl groups per glycoside unit in equatorial positions 2 and 3 that can be oxidized to form two aldehyde groups with cleavage of the C2–C3 bond (Figure S2, step 1, Supporting Information) by sodium periodate, as the oxidizing agent. Next, the obtained aldehyde groups react with EDA at pH 5.5 to form the imines (Schiff bases) that are readily and selectively reduced by sodium cyanoborohydride as reducing agent (Figure S2, step 2 and 3, Supporting Information). The oxidation of glucoside units (step 1) on PG NPs by sodium periodate is quantitative,[18] Therefore, the oxidation of 20% units results in the formation of 40% aldehyde groups. However, the conversion of aldehydes to imine and amine groups (step 2 and 3) is less efficient and therefore some aldehyde groups can be reduced to alcohol groups during the reduction reaction. To give an insight into the chemical structure of PG_{EDA} NPs and the mechanism of reaction, ^{1}H and ^{1}H–^{13}C HSQC and ^{13}C solid-state nuclear magnetic resonance (NMR) analysis were performed. The degree of substitution (percentage by moles of glycoside units of glycogen effectively modified) of the PG NPs by EDA was ≈19%, as determined by ^{1}H NMR spectroscopy (Figure S3, Supporting Information) and deconvolution of EDA peaks in the range 2.7–3 ppm. (Figure S4, Supporting Information). As no evidence of unreacted aldehydes was observed by NMR in the range of 10 ppm, these results suggest that 21% aldehydes are ultimately reduced to hydroxyl groups. Therefore, the functionalized glycoside units in the obtained PG_{EDA} NPs can bear either one or two EDA moieties, as shown in Figure S2 (Supporting Information).

Interestingly, the degree of substitution of the PG NPs by EDA of ≈19% was also confirmed by the analysis of ^{13}C solid state NMR spectra (Figure S5, Supporting Information). It is worth noting that PG_{EDA} is a highly branched dendrimer-like nanoparticle with a high molecular weight of 18 MDa.[17] Inside the nanoparticle, the rigid inner chains may be unobservable by high-resolution NMR in solution because of the slower tumbling of protons, which results in the broadening of peaks. In contrast, ^{13}C solid-state NMR spectrum enables probing the chemical modification of PG NPs both in the outer and inner chains. The comparison of the results obtained by the liquid

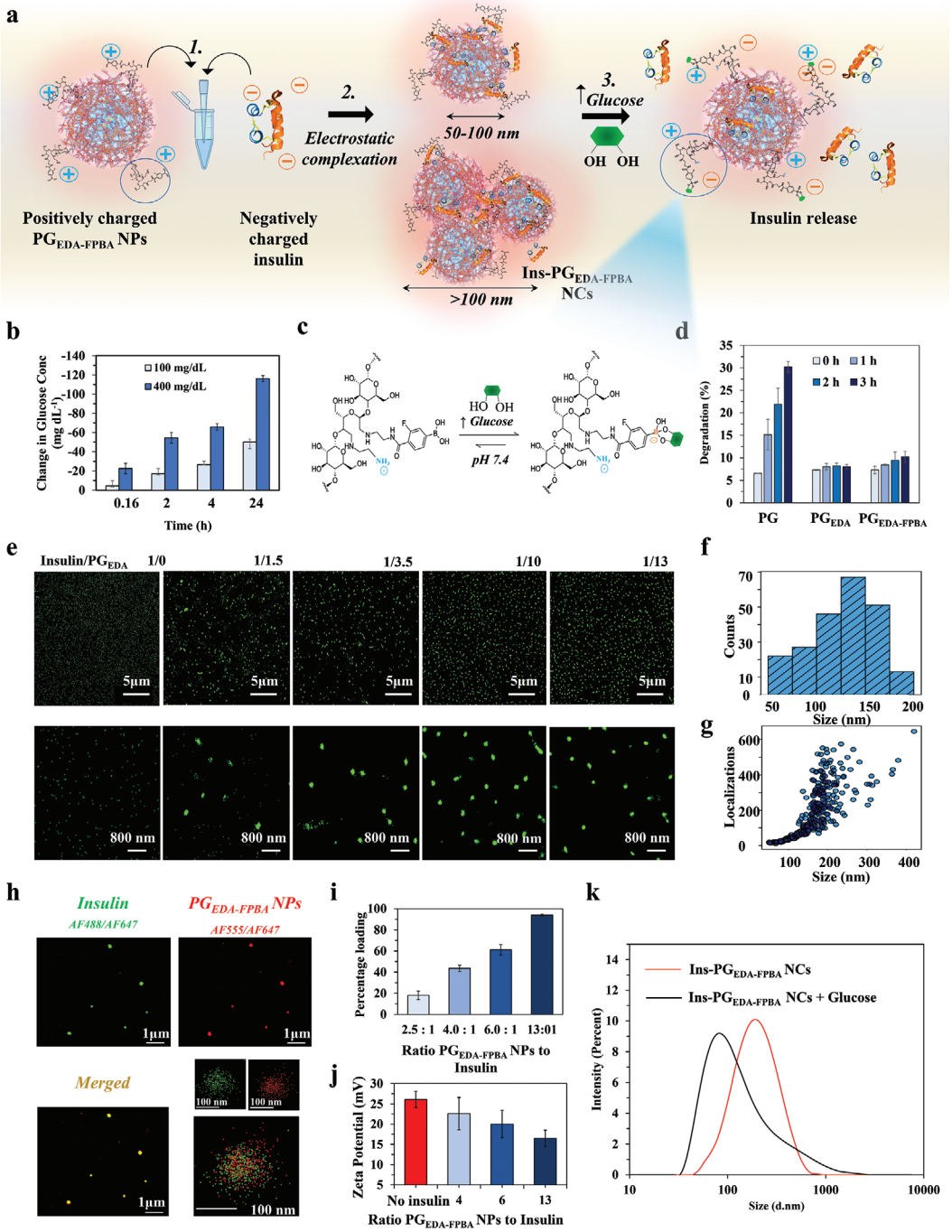

Figure 1. Charge-switchable nanosugars for glucose-responsive insulin release. a) Schematic showing the complexation of positively charged $PG_{EDA-FPBA}$ NPs with negatively charged insulin through electrostatic interactions the morphologies of the nanocomplexes (1. and 2.) and the mechanism of release of insulin when $PG_{EDA-FPBA}$ NCs are incubated with glucose (3.). b) Glucose-binding ability of $PG_{EDA-FPBA}$ NPs. The particles were incubated in glucose solutions (100 or 400 mg dL^{-1}), and the concentration of glucose in the supernatant was analyzed at different times. c) Schematic showing the esterification of FPBA groups with glucose at pH 7.4 leading to a reduction of positive charge on $PG_{EDA-FPBA}$ NP. d) Comparison of the degradation yield of PG NPs, PG_{EDA} NPs, and $PG_{EDA-FPBA}$ NPs by α-amylase. The extent of degradation of the PG-based particles by α-amylase as a function of time was determined using the Somogyi–Nelson assay. e) STORM images of Ins-$PG_{EDA-FPBA}$ NCs obtained at different weight ratios of FITC-insulin/$PG_{EDA-FPBA}$ NPs. f) Size distribution of Ins-$PG_{EDA-FPBA}$ NCs prepared at FITC-insulin/$PG_{EDA-FPBA}$ NP ratio of 1:13. g) Scatter plot of localizations versus size of Ins-$PG_{EDA-FPBA}$ NCs prepared at an insulin-to-$PG_{EDA-FPBA}$ NP weight ratio of 1:13. h) Multicolor STORM images of Ins-$PG_{EDA-FPBA}$ NCs, where insulin was dual labeled with AF488/AF647 and $PG_{EDA-FPBA}$ NPs were dual labeled with AF555/AF647. The colocalization signal confirms the efficient binding of insulin to the $PG_{EDA-FPBA}$ NPs. and magnified STORM images of single Ins-$PG_{EDA-FPBA}$ NC. i) Efficiency of loading of insulin onto $PG_{EDA-FPBA}$ NPs. j) Changes in ζ-potential of $PG_{EDA-FPBA}$ NPs after complexation with insulin at different ratios. k) Size distribution of Ins-$PG_{EDA-FPBA}$ NCs determined by DLS with and without the addition of glucose (400 mg dL^{-1}). The error bars represent the mean ± standard deviation (SD) (n = 3 per group).

and solid NMR analysis indicates that the branched polysaccharide chains of PG_{EDA} NPs are not stiff and the high-resolution NMR in solution can probe the whole nanoparticles. In principle the reductive amination of glucose residues occurs both on the outer and inner polysaccharide chains of PG_{EDA} NPs. However, a high positive zeta potential value of 40 mV was measured on PG_{EDA} NPs (Figure S1d, Supporting Information), this suggests that the amine groups were introduced primarily on the outer shell of the nanoparticles to confer a high surface charge density.

Next activated FPBA in the form of *N*-hydroxysuccinimide ester was linked to the primary amine of PG_{EDA} NPs (Figure S6, Supporting Information). It is worth mentioning that boronic acids typically bind to *cis*-1,2- or 1,3-diols to form reversible five- or six-membered cyclic esters.[19] The glycoside units in PG NP do not exhibit *cis*-1,2- or 1,3-diols, hence FPBA does not have affinity for the polysaccharide chains.

The degrees of substitution of the PG NPs by FPBA was 10% as determined by NMR (Figure S7, Supporting Information) and ultraviolet–visible (UV–vis) spectroscopy (Figure S8, Supporting Information). Therefore, the ratio between the primary amines of EDA and FPBA groups on the modified $PG_{EDA\text{-}FPBA}$ NPs was 1.9. The amidation reaction by FPBA groups (pK_a 7.2) led to a significant reduction of the positive charge density on $PG_{EDA\text{-}FPBA}$ NPs from 40 mV (PG_{EDA} NPs) to 25 mV (Figure S1d, Supporting Information)

The hydrodynamic diameters of PG_{EDA} NPs and $PG_{EDA\text{-}FPBA}$ NPs (Figure S1c, Supporting Information) increased by ≈25% relative to that of the unmodified PG NPs. TEM images revealed a significant size shrinkage of the $PG_{EDA\text{-}FPBA}$ NPs upon drying to ≈34 ± 10 nm (Figure S9, Supporting Information), indicating that the $PG_{EDA\text{-}FPBA}$ NPs were highly hydrated. The binding of the $PG_{EDA\text{-}FPBA}$ NPs to glucose by esterification with the FPBA moieties was evaluated as a function of time after the addition of glucose at clinically relevant glucose concentrations of 100 mg dL ^{1} (5.6 mmol L^{-1}) and 400 mg dl^{-1} (22.2 mmol L^{-1}) in phosphate-buffered saline (PBS) pH 7.4 (Figure 1b). The concentration of glucose in the supernatants of the original glucose solutions of 100 and 400 mg dL^{-1} decreased by ≈50 and 120 mg dL^{-1}, respectively, after 24 h, reflecting the effective binding of glucose to the $PG_{EDA\text{-}FPBA}$ NPs.

In agreement with these results, the ζ-potential of the $PG_{EDA\text{-}FPBA}$ NPs decreased from 25 mV in the absence of glucose to ≈15 mV after 24 h incubation with 400 mg dL^{-1} glucose at pH 7.4. The binding of glucose to FPBA groups has been reported to induce a decrease in the pK_a (≈6.4) of boronic acid[11,13–15,20] and therefore, a shift of the equilibrium toward the boronate form (Figure 1c). Consequently, the negative charges arising from the boronate moieties reduced the positive charge density on the $PG_{EDA\text{-}FPBA}$ NPs. The biodegradability of the $PG_{EDA\text{-}FPBA}$ NPs by α-amylase, which is typically present in plasma, was measured in vitro. Compared to the unmodified PG NPs (Figure 1d), $PG_{EDA\text{-}FPBA}$ NPs exhibited minimal degradation (8–10%) during incubation with α-amylase for 3 h, as determined using the Somogyi–Nelson amylolytic enzyme activity assay (Figure 1d). The stability of the $PG_{EDA\text{-}FPBA}$ NPs against α-amylase was also confirmed by fluorescence correlation spectroscopy (FCS) and STORM imaging where the diffusion coefficient and corresponding radius of the Alexa Fluor (AF) 555 (AF555)-labeled $PG_{EDA\text{-}FPBA}$ NPs showed minimal changes in the presence of the hydrolytic enzyme (Figure S10a,b, Supporting Information).

However, the $PG_{EDA\text{-}FPBA}$ NPs were partially degradable (40%) when treated for 3 h with β-amylase, mimicking lysosomal enzymes (Figure S10c, Supporting Information). This result suggests that upon cellular uptake and intracellular trafficking, the lysosomal exo-amylases can break down the $PG_{EDA\text{-}FPBA}$ NPs. Overall, those results indicate that the engineered $PG_{EDA\text{-}FPBA}$ NPs exhibit affinity for glucose under the relevant blood glucose concentration observed in diabetes (400 mg dL^{-1}) and likely maintain their structural integrity in the extracellular environment when injected in the bloodstream or subcutaneously.

Next, the electrostatic interactions between the positively charged $PG_{EDA\text{-}FPBA}$ NPs and negatively charged insulin (isoelectric point of 5.3) were exploited to obtain glucose-responsive Ins-$PG_{EDA\text{-}FPBA}$ NCs (Figure 1a). As the binding of glucose to the FPBA moieties causes a decrease in the positive charge density on the $PG_{EDA\text{-}FPBA}$ NPs (Figure 1c), we hypothesize that this condition can weaken the attraction between insulin and the $PG_{EDA\text{-}FPBA}$ NPs to stimulate insulin release. To gain a deeper insight into the morphology of individual NCs at a molecular level, the complexation process was investigated by single molecules localization microscopy STORM. The Ins-$PG_{EDA\text{-}FPBA}$ NCs were prepared using fluorescein isothiocyanate (FITC)-labeled insulin at different FITC-labeled insulin-to-$PG_{EDA\text{-}FPBA}$ NPs weight ratios (1:0, 1:1.5, 1:3.5, 1:10, and 1:13), where the concentration of insulin was fixed at 1 mg mL^{-1}. Naked insulin molecules (free insulin without association with NPs) or Ins-$PG_{EDA\text{-}FPBA}$ NCs were deposited on a glass coverslip for STORM-total internal reflection fluorescence imaging (Figure 1e). The list of localizations was processed using a clustering analysis script to quantitatively estimate the number of localizations inside a single NC and the size of the NCs. Notably, the number of localizations is proportional to the number of insulin molecules. At low ratios (1:1.5, 1:3.5), free insulin molecules were imaged (Figure 1e), while with increasing weight ratios up to 1:13, the free insulin molecules originally visualized in the background gradually disappeared and only round NCs of 160 ± 40 nm in size were detected (Figure 1e,f). This result indicates that all insulin molecules (1 mg) have been incorporated into $PG_{EDA\text{-}FPBA}$ NPs (13 mg). Figure 1g shows that the number of localizations detected within a single NC obtained at the ratio of 1:13 increases with the diameter of the NC. A limited number of localizations, ranging from 15 to 50, were detected on the small NCs (50–100 nm), whereas heterogeneous clusters of molecules ranging from 80 to 600 were observed in the larger NCs (100–300 nm). Hence, STORM imaging analysis allows the elucidation of the morphologies of the NCs, suggesting that the insulin molecules can either deposit on the brushed charged surface of individual Ins-$PG_{EDA\text{-}FPBA}$ NCs to form smaller NCs or remain embedded between multiple Ins-$PG_{EDA\text{-}FPBA}$ NCs to form larger NCs (Figure 1a); this is also evident by TEM analysis (Figure S11, Supporting Information). Multicolor STORM imaging was employed to verify the colocalization between insulin molecules and the $PG_{EDA\text{-}FPBA}$ NPs and confirmed the efficient loading of insulin molecules onto the $PG_{EDA\text{-}FPBA}$ NPs (Figure 1h). The maximum insulin loading capacity (95%) of the $PG_{EDA\text{-}FPBA}$ NPs was calculated by fluorescence analysis of the

Ins-$PG_{EDA\text{-}FPBA}$ NCs after spin filtration of the unbound insulin at increasing $PG_{EDA\text{-}FPBA}$ NPs-to-insulin weight ratios (Figure 1i and Figure S12, Supporting Information). The charge of the Ins-$PG_{EDA\text{-}FPBA}$ NCs was reduced from 25 to 15 mV at the insulin-to-$PG_{EDA\text{-}FPBA}$ NPs weight ratios 1:13. This reduction in surface charge indicates that complexation is primarily mediated by electrostatic interactions (Figure 1j) and likely by an increase in entropy due to the release of counterions and coordinated water molecules. The increase in size of the $PG_{EDA\text{-}FPBA}$ NPs to 160 ± 70 upon binding to insulin was also confirmed by DLS measurements (Figure 1k). NMR spectra of the Ins-$PG_{EDA\text{-}FPBA}$ NCs confirmed that insulin was immobilized (insulin peaks disappear) in the complex by electrostatic interactions with the amine groups (Figure S13, Supporting Information). The Ins-$PG_{EDA\text{-}FPBA}$ NCs maintained their colloidal stability and size after storage for 6 months.

2.2. In Vitro and Ex Vivo Glucose-Responsive and Pulsatile Release of Insulin

The kinetics of insulin release from the glucose-responsive Ins-$PG_{EDA\text{-}FPBA}$ NCs (**Figure 2**a) was investigated in vitro under normal (100 mg dL^{-1}) and elevated blood glucose (400 mg dL^{-1}) concentrations. Ins-$PG_{EDA\text{-}FPBA}$ NCs loaded with 2 IU insulin ($PG_{EDA\text{-}FPBA}$/ insulin = 13/1) showed rapid insulin release at elevated glucose levels with ≈70% of the payload released after 4 h. In contrast, under no glucose (PBS alone) and normal blood glucose concentration conditions (100 mg dL^{-1}), only 20% and 30% of the loaded insulin was released, respectively (Figure 2a). The disassembly of the Ins-$PG_{EDA\text{-}FPBA}$ NCs upon glucose incubation was confirmed by a shift in the size distribution of the NCs (Figure 1k). For comparison, when the insulin release was monitored under the same experimental conditions from a non-glucose-responsive NCs, obtained by the electrostatic association of insulin with PG_{EDA} NPs (Ins-PG_{EDA} NCs), a very slow and glucose-insensitive insulin release was observed (Figure 2b). In addition, Ins-$PG_{EDA\text{-}FPBA}$ NCs further enabled pulsatile insulin release in vitro for up to three cycles by switching the glucose concentrations between 100 and 400 mg dL^{-1} (Figure 2c). Moreover, the released insulin phosphorylated AKT (p-AKT) in HepG2 liver cells (Figure 2d), confirming its bioactivity in vitro. Cytotoxicity assays on fibroblasts (3T3) and macrophages, representing the primary cell types that reside in the SC connective tissues,[21] found no toxicity following exposure to the $PG_{EDA\text{-}FPBA}$ NPs for up to 96 h (Figure S14, Supporting Information). Overall, these results suggest that the engineered Ins-$PG_{EDA\text{-}FPBA}$ NCs are non-toxic and have the potential to rapidly respond to dynamic glucose changes in vivo in the SC tissue by deploying fully bioactive insulin.

Ex vivo, insulin release from Ins-$PG_{EDA\text{-}FPBA}$ NCs incubated in normal plasma for 2 h was ≈18% of the total insulin loaded (Figure 2e), in agreement with the in vitro results (Figure 2a). However, the percentage of insulin released in "diabetic plasma" (addition of glucose to normal plasma) after 2 h incubation was lower than that observed in vitro (25%; Figure 2e vs 55%; Figure 2a). This suggests that the adsorption of plasma proteins onto the Ins-$PG_{EDA\text{-}FPBA}$ NCs (i.e., a protein corona) may hinder and slow the release of insulin in vivo. This was confirmed by insulin release studies from Ins-$PG_{EDA\text{-}FPBA}$ NCs in the presence of human serum albumin (Figure S15, Supporting Information). Whole blood analysis following SC injection of fluorescently labeled $PG_{EDA\text{-}FPBA}$ NPs in Wild-type (WT) C57BL/6 mice demonstrated that most of the $PG_{EDA\text{-}FPBA}$ NPs were associated with the peripheral blood mononuclear cells (PBMCs), with a fraction of the $PG_{EDA\text{-}FPBA}$ NPs still visible in the plasma (Figure 2f,g). The thermal stability of insulin, either "naked" or embedded into Ins-$PG_{EDA\text{-}FPBA}$ NCs, was then studied by monitoring the heat-induced aggregation and changes in the secondary structure of insulin. The monomeric insulin band disappeared after incubation for 24 h at 60 °C due to insulin aggregation, whereas Ins-$PG_{EDA\text{-}FPBA}$ NCs preserved insulin in its active monomeric state (Figure 2h). Furthermore, a change in the secondary structure was observed by circular dichroism (CD) analysis for naked insulin after heat treatment for 1 h at 60 °C, whereas the structure of insulin attached to the NCs (Ins-$PG_{EDA\text{-}FPBA}$ NCs) remained unchanged (Figure 2i). Thus, the Ins-$PG_{EDA\text{-}FPBA}$ NCs formulation could potentially improve diabetes care in resource-poor settings where there is a reduced capacity to avoid insulin exposure to high temperatures.[22]

2.3. In Vivo Blood Glucose Regulation in Two Distinct Diabetic Mouse Models

To evaluate the therapeutic properties of Ins-$PG_{EDA\text{-}FPBA}$ NCs in vivo, we employed two distinct insulin-deficient mouse models: (1) the spontaneously type 1 diabetic Akita mouse model (C57BL/6-Ins2-Akita/J), in which a mutation in the proinsulin gene causes insulin misfolding and beta cell degeneration,[23] and (2) the widely used streptozotocin (STZ)-induced diabetic mouse model. [11] Akita mice and STZ-induced diabetic mice were randomly grouped and subcutaneously injected with either Ins-$PG_{EDA\text{-}FPBA}$ NCs (insulin dose 80 IU kg^{-1}) or naked insulin (16 IU kg^{-1}) as appropriate control. Both naked insulin and Ins-$PG_{EDA\text{-}FPBA}$ NCs triggered a rapid decrease of the elevated blood glucose level (BGL) (500–600 mg dL^{-1}) in the treated diabetic mice (both Akita and STZ-induced diabetic mice) to reach normoglycemia (<200 mg dL^{-1}) within 30–40 min (**Figure 3**a and **4**a). These results indicate that the injected Ins-$PG_{EDA\text{-}FPBA}$ NCs can rapidly sense and reduce the high concentration of interstitial glucose in these diabetic mice, as the NCs can promptly deploy bioactive insulin in the SC injection site that directly enters the blood stream. When $PG_{EDA\text{-}FPBA}$ NPs (without loaded insulin) were injected as a control, a slight decrease in BGL was induced in the diabetic Akita mice (Figure 3a), possibly a result of glucose binding to the boronate moieties (Figure 1b). Ins-$PG_{EDA\text{-}FPBA}$ NCs maintained normoglycemia for 13.5 h, whereas naked insulin maintained the blood glucose at a normal level for 3 h only in both the Akita and STZ-induced diabetic mice (Figure 3b and 4b). Additionally, plasma insulin analysis by enzyme-linked immunosorbent assay (ELISA) revealed a rapid insulin release, with a peak plasma insulin level of ≈700 and 950 μU mL^{-1} in 1 h post- Ins-$PG_{EDA\text{-}FPBA}$ NCs administration to the Akita and STZ-induced diabetic mice, respectively (Figure 3c and 4c); this result is consistent and correlated with the rapid decrease in BGL observed in those

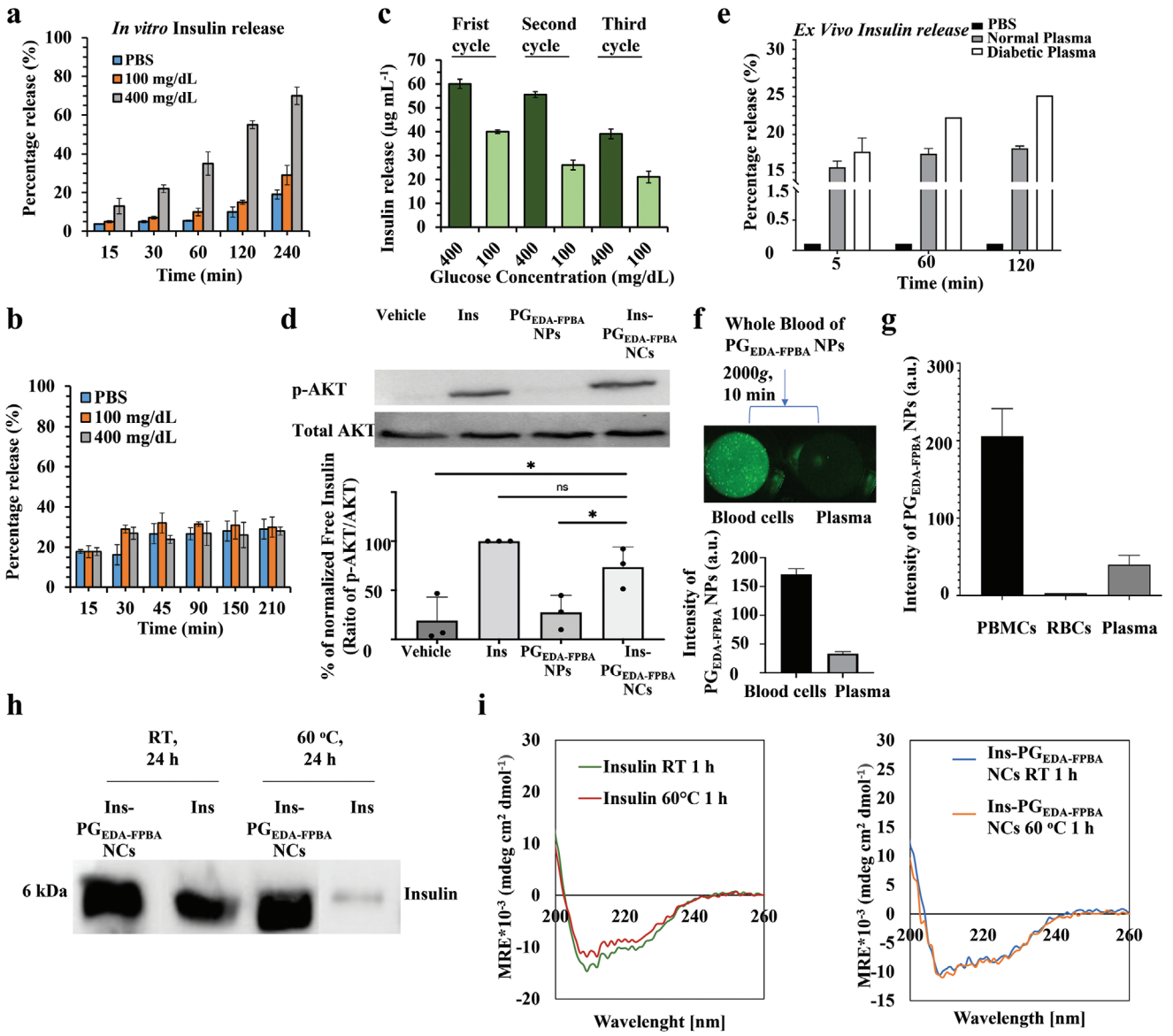

Figure 2. Characterization of glucose-dependent insulin release of nanosugars. a) Release kinetics of insulin from Ins-$PG_{EDA\text{-}FPBA}$ NCs in PBS and at different glucose concentrations. b) Release kinetics of insulin from Ins-PG_{EDA} NCs in PBS and at different glucose concentrations. The complexes were prepared in 10 mM PBS at pH 6.5 and FITC-labeled insulin was used. c) Pulse insulin release from Ins-$PG_{EDA\text{-}FPBA}$ NCs by alternate addition of glucose at 100 and 400 mg dL^{-1}. The complex was incubated in each solution for 5 min. d) Western blot analysis of p-AKT in starved HepG2 cells after 15 min of exposure to vehicle (Milli-Q water), free insulin, $PG_{EDA\text{-}FPBA}$ NPs, or Ins-$PG_{EDA\text{-}FPBA}$ NCs. The concentration of insulin was the same across all groups (100 nM). Pan-AKT was used as the loading control and the ratio of p-AKT over total AKT was quantified. Data are expressed as mean ± standard error of the mean and consist of three replicates. * $p < 0.05$, ns denotes $p > 0.05$. e) Quantification of blood insulin in human normal and diabetic PPP via ELISA. Percentage of insulin released from Ins-$PG_{EDA\text{-}FPBA}$ NCs in normal and diabetic PPP (ex vivo) measured over 2 h. f) Distribution of $PG_{EDA\text{-}FPBA\text{-}Cy5.5}$ NPs in blood cells and plasma post SC injection in C57BL/6 mice. g) Distribution of $PG_{EDA\text{-}FPBA\text{-}Cy5.5}$ NPs in PBMCs, red blood cells (RBCs), and plasma post SC injection in C57BL/6 mice. h) Western blot analysis of insulin stability in insulin and Ins-$PG_{EDA\text{-}FPBA}$ NCs groups at room temperature (RT) and 60 °C for 24 h. i) CD analysis of changes in the structure of insulin in insulin and Ins-$PG_{EDA\text{-}FPBA}$ NCs groups at RT and 60 °C for 1 h. The error bars represent the mean ± SD (n = 3 per group).

diabetic mice (Figure 3a and 4a). Subsequently, the plasma insulin level decreased considerably to 39 μU mL^{-1} within 4 h in the Akita diabetic mice due to the pharmacological elimination of insulin. A sustained insulin release was observed for up to 13 h when Ins-$PG_{EDA\text{-}FPBA}$ NCs were injected in both the Akita and STZ-induced diabetic mice. In contrast, both Akita and STZ-induced mice treated with naked insulin showed a spike in plasma insulin level at 1 h after injection (1500 and 1600 μU mL^{-1}, respectively), followed by a steep fall to undetectable levels of insulin within 4 h (Figure 3c and 4c). To further verify the in vivo efficacy of Ins-$PG_{EDA\text{-}FPBA}$ NCs in responding to a glucose challenge mimicking a meal, we performed an intraperitoneal glucose tolerance test (IPGTT, 1.5 g kg^{-1} glucose) in both the Akita and STZ-induced diabetic mice 4 h after

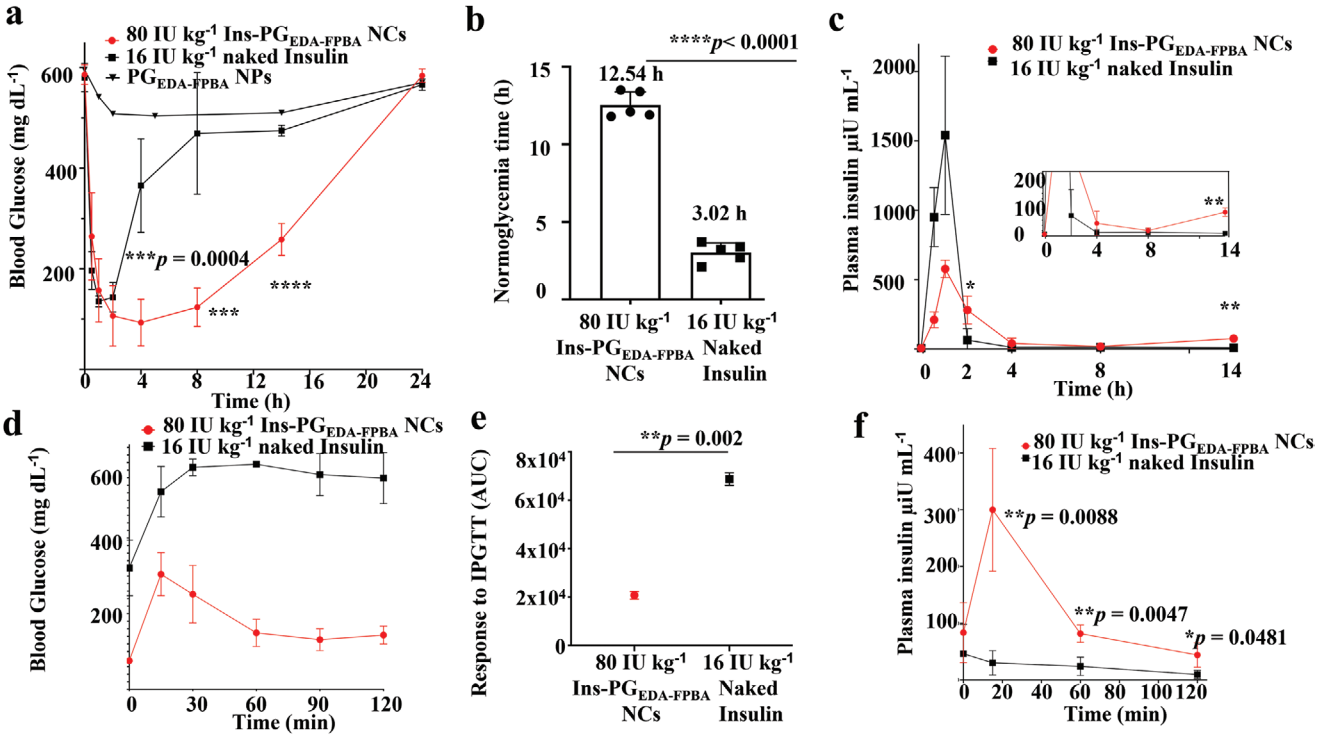

Figure 3. In vivo evaluation of Ins-$PG_{EDA\text{-}FPBA}$ NCs injection in an Akita spontaneous type 1 diabetic mouse model. a) Blood glucose level (BGL) in Akita type 1 diabetic mice after treatment with naked insulin (insulin dose 16 IU kg^{-1}, $n = 5$), Ins-$PG_{EDA\text{-}FPBA}$ NCs (insulin dose 80 IU kg^{-1}, $n = 5$), or $PG_{EDA\text{-}FPBA}$ NPs (36 mg kg^{-1}, $n = 1$). Data are mean ± SD. b) Duration of normoglycemic conditions maintained in Akita diabetic mice treated with subcutaneously injected naked insulin or Ins-$PG_{EDA\text{-}FPBA}$ NCs (insulin dose 80 IU kg^{-1}) ($n = 5$). c) Concentration of plasma insulin (quantified by insulin ELISA kit) in Akita diabetic mice treated with naked insulin (insulin dose 16 IU kg^{-1}, $n = 3$) or Ins-$PG_{EDA\text{-}FPBA}$ NCs (insulin dose 80 IU kg^{-1}, $n = 3$). Inset: magnified view of data at 14 h post-treatment. $p < 0.01$. d) IPGTT results of Akita diabetic mice at 4 h after treatment with Ins-$PG_{EDA\text{-}FPBA}$ NCs (insulin 80 IU kg^{-1}) or naked insulin (insulin dose 16 IU kg^{-1}). The glucose dose was set to 1.5 g kg^{-1}; $n = 3$–4. e) AUC of IPGTT response at 120 min, with the baseline set at the 0–min blood glucose reading ($n = 3$–4). f) In vivo glucose-responsive insulin release triggered by intraperitoneal glucose injection at 4th h after treatment with naked insulin (insulin dose 16 IU kg^{-1}) or Ins-$PG_{EDA\text{-}FPBA}$ NCs (insulin dose 80 IU kg^{-1}), as quantified using an insulin ELISA kit; the glucose dose was set to 1.5 g kg^{-1} ($n = 3$–4). All statistical analyses were performed by ANOVA with a Tukey post hoc test or Student's *t*-test. *$p < 0.05$, **$p < 0.01$, ***$p < 0.001$. The error bars represent the mean ± SD.

treatment with naked insulin or Ins-$PG_{EDA\text{-}FPBA}$ NCs. In response to the IPGTT, the mice receiving naked insulin rapidly returned to their initial hyperglycemic state (Figure 3d and 4d). Conversely, mice treated with Ins-$PG_{EDA\text{-}FPBA}$ NCs, an initial increase of BGL to 240 mg dL^{-1} was robustly controlled to a BGL to normal range (<200 mg dL^{-1}) up to 2 h after the IPGTT (Figure 3d, e and Figure 4d, e). The area under the curve (AUC) shown in Figure 3e and 4e was used to compare the responsiveness to IPGTT after administration of naked insulin or Ins-$PG_{EDA\text{-}FPBA}$ NCs in the Akita and STZ-induced diabetic mice. The glycemic control in mice treated with Ins-$PG_{EDA\text{-}FPBA}$ NCs was associated with a significant spike in plasma insulin from 60 to 220 µU mL^{-1} in the Akita mice and from 30 to 320 µU mL^{-1} in the STZ-induced diabetic mice, respectively (Figure 3f and 4f). This is while mice treated with naked insulin showed no significant change in the plasma insulin level upon IPGTT, as expected (Figure 3f and 4f). Overall, our data in the two insulin-deficient diabetic mouse models show that SC injection of Ins-$PG_{EDA\text{-}FPBA}$ NCs in diabetic mice enabled a rapid insulin release under the hyperglycemic conditions at high glucose levels at the local injection site and a sustained insulin release under normal low glucose levels. Normoglycemic conditions were maintained by Ins-$PG_{EDA\text{-}FPBA}$ NCs up to 13 h post-administration through an early-stage rapid insulin release and a later-stage basal insulin release kinetics profile, while avoiding both severe hypoglycemia and transient hyperglycemia. In addition, Ins-$PG_{EDA\text{-}FPBA}$ NCs showed a rapid and efficient response to a glucose challenge, providing extended glycemic control in vivo when compared to naked insulin.

2.4. Unravelling the Mechanism of Insulin Release and the Fate of Ins-$PG_{EDA\text{-}FPBA}$ NCs

To shed light on the underlying mechanism of insulin release from Ins-$PG_{EDA\text{-}FPBA}$ NCs and the fate of Ins-$PG_{EDA\text{-}FPBA}$ NCs in vivo, pharmacokinetic studies of the glucose-responsive Ins-$PG_{EDA\text{-}FPBA}$ NCs (lymphatic absorption and trafficking, systemic circulation and blood clearance, tissue distribution, extravasation, and excretion) were performed in both the Akita mice and STZ-induced diabetic mice after SC injection of the NCs. The in vivo biosafety of the engineered $PG_{EDA\text{-}FPBA}$ NPs, administrated SC, was first assessed and showed a survival rate of 100%, with no significant weight loss or any signs of illness for 7 days post-delivery (Figure S16, Supporting Information). Next, the mice were subcutaneously administered either labeled

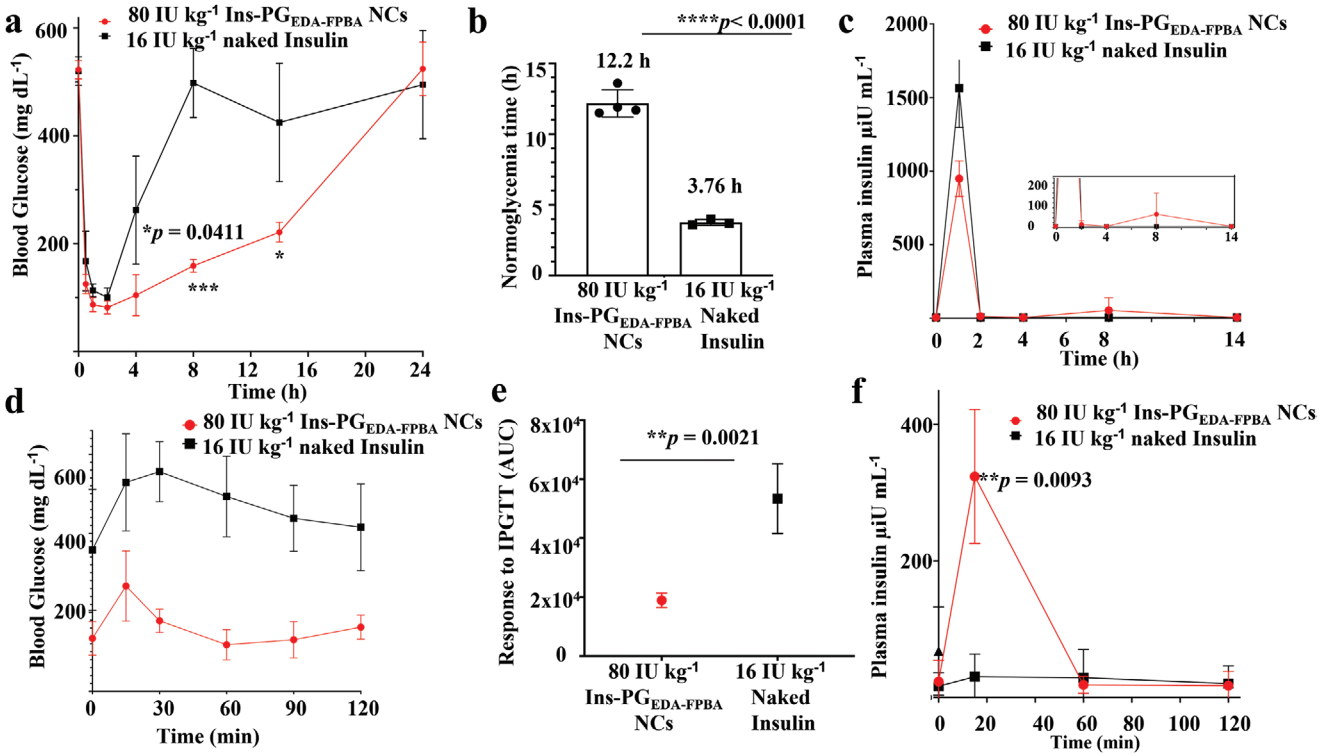

Figure 4. In vivo evaluation of Ins-$PG_{EDA\text{-}FPBA}$ NCs injection in an STZ-induced diabetic mouse model. a) Blood glucose concentration in STZ-induced diabetic mice (n = 3–4). b) Duration of normoglycemic conditions maintained in STZ-induced diabetic mice treated with subcutaneously injected naked insulin (insulin dose 16 IU kg^{-1}) or Ins-$PG_{EDA\text{-}FPBA}$ NCs (insulin dose 80 IU kg^{-1}) (n = 3–4). c) Concentration of plasma insulin (n = 3) in STZ-induced diabetic mice after treatment with naked insulin (insulin dose 16 IU kg^{-1}) or Ins-$PG_{EDA\text{-}FPBA}$ NCs (insulin dose 80 IU kg^{-1}). Data are mean ± SD (n = 3). d) IPGTT results of STZ-induced diabetic mice at 4th h after treatment with Ins-$PG_{EDA\text{-}FPBA}$ NCs (insulin dose 80 IU kg^{-1}) or naked insulin (insulin dose 16 IU kg^{-1}). The glucose dose was set to 1.5 g kg^{-1}; n = 3–4. e) AUC of IPGTT response at 120th min, with the baseline set at the 0–min blood glucose reading (n = 3–4). f) In vivo glucose-responsive insulin release triggered by intraperitoneal glucose injection at 4th h after treatment with naked insulin (insulin dose 16 IU kg^{-1}) or Ins-$PG_{EDA\text{-}FPBA}$ NCs (insulin dose 80 IU kg^{-1}), as quantified using an insulin ELISA kit; the glucose dose was set to 1.5 g kg^{-1} (n = 3–4). The error bars represent the mean ± SD. All statistical analyses were performed by ANOVA with a Tukey post hoc test or Student's t-test. *p < 0.05, **p < 0.01, ***p < 0.001.

Ins-$PG_{EDA\text{-}FPBA\text{-}Cy5.5}$ NCs, naked insulin as control (**Figure 5**a), dual-labeled $Ins_{\text{-}Cy7.5}$-$PG_{EDA\text{-}FPBA\text{-}Cy5.5}$ NCs, naked $Ins_{\text{-}Cy7.5}$, or $PG_{EDA\text{-}FPBA\text{-}Cy5.5}$ NP in Akita mice (Figure 5b). Super-resolution microscopy imaging combined with an Odyssey near-infrared fluorescence (NIRF) scanning was used to monitor the presence of Ins-$PG_{EDA\text{-}FPBA}$ NCs and insulin in the organs and blood. In 24 h post-injection, mice were humanely killed, and vital organs (heart, liver, spleen, lung, kidney, and brain), skin, and muscle were isolated for ex vivo fluorescence imaging to determine sample biodistribution (Figure 5a,b). Representative Odyssey images of Akita diabetic mice (Figure 5a) and STZ-induced diabetic mice (Figure S17, Supporting Information) showed a prolonged retention (24 h post-injection) of Ins-$PG_{EDA\text{-}FPBA\text{-}Cy5.5}$ NCs in the proximity of the injection site (i.e., under the skin). Significant accumulation of Ins-$PG_{EDA\text{-}FPBA\text{-}Cy5.5}$ NCs in the liver and kidneys was observed 24 h post-injection (Figure 5a), with only limited retention after 96 h (Figure S18, Supporting Information) and no uptake into the spleen, lung, heart, or brain. A similar biodistribution of the dual-labeled sample $Ins_{Cy7.5}$-$PG_{EDA\text{-}FPBA\text{-}Cy5.5}$ NCs was demonstrated (Figure 5b) as well as a comparable biodistribution of the $PG_{EDA\text{-}FPBA\text{-}Cy5.5}$ NPs was observed in Akita mice (Figure 5b) and WT C57BL/6 mice (Figure S19a, Supporting Information). Importantly, the analysis of all organs 16 weeks post-injection (Figure S19a, Supporting Information) in WT C57BL/6 mice revealed complete elimination of the injected $PG_{EDA\text{-}FPBA\text{-}Cy5.5}$ NPs from the liver and kidneys with a low signal still present at the injection site (Figure S19a, Supporting Information).

The blood clearance of Ins-$PG_{EDA\text{-}FPBA\text{-}Cy5.5}$ NCs or $PG_{EDA\text{-}FPBA\text{-}Cy5.5}$ NPs was then monitored in Akita mice (Figure 5c) and healthy C57BL/6 mice (Figure S19b, Supporting Information). Fluorescence signal spikes of Ins-$PG_{EDA\text{-}FPBA\text{-}Cy5.5}$ NCs or $PG_{EDA\text{-}FPBA\text{-}Cy5.5}$ NPs, corresponding to 1% of injected dose, were observed in the blood 2 h post-injection. A second peak corresponding to 1.5% of the injected dose was observed ≈24 h post-injection, followed by a progressive decrease in the signal up to 96 h (where 0.5% of injected dose remained) (Figure 5c). The initial spikes at 2 h post injection can be attributed to the onset of vascular endothelial dysfunction that is typically observed in Akita mice.[24] This was confirmed by the contrasting results obtained in healthy C57BL/6 mice, where a gradual increase in circulating Ins-$PG_{EDA\text{-}FPBA\text{-}Cy5.5}$ NPs was detected in the first 2 h post-injection (Figure S19b, Supporting Information). These data reveal that both Ins-$PG_{EDA\text{-}FPBA}$ NCs and $PG_{EDA\text{-}FPBA}$ NPs readily enter the blood stream upon SC administration. Yet, unlike insulin monomers and dimers that

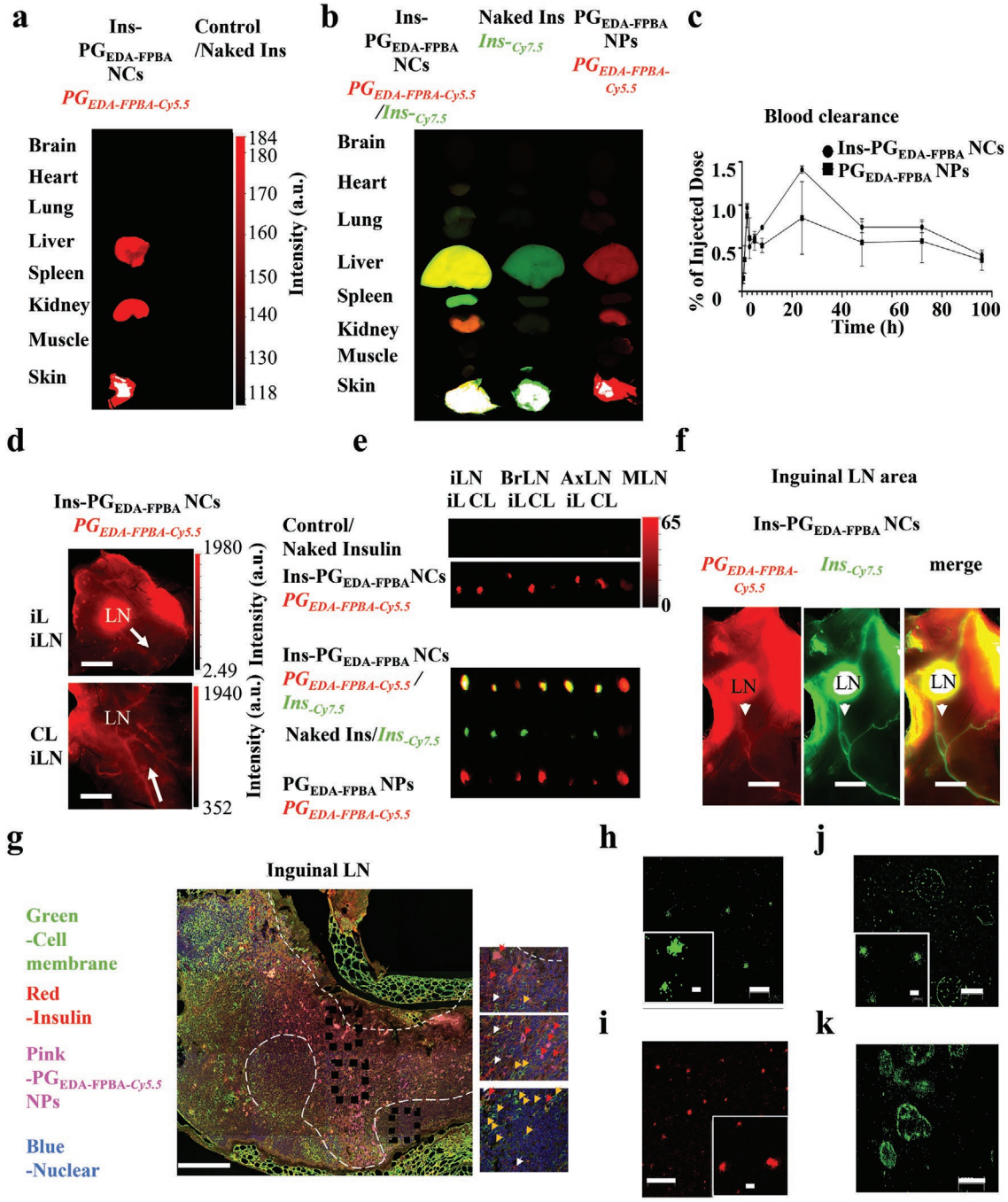

Figure 5. Biodistribution and lymphatic pathway uptake and hepatobiliary exertion pathway of Ins-$PG_{EDA\text{-}FPBA}$ NCs post SC injection. a) Representative NIRF scans of perfused organs from Akita mice collected at 24th h after SC injection of Ins-$PG_{EDA\text{-}FPBA\text{-}Cy5.5}$ NCs (36 mg kg^{-1}) or control (unlabeled naked insulin, insulin dose 16 IU kg^{-1}). b) Representative NIR fluorescence scans of perfused organs from Akita mice collected at 24th h after SC injection of $Ins_{\text{-}Cy7.5}$-$PG_{EDA\text{-}FPBA\text{-}Cy5.5}$ NCs (insulin dose 80 IU kg^{-1}), naked $Ins_{\text{-}Cy7.5}$ (insulin dose 16 IU kg^{-1}), or $PG_{EDA\text{-}FPBA\text{-}Cy5.5}$ NPs (36 mg kg^{-1}). c) Blood clearance of Ins-$PG_{EDA\text{-}FPBA\text{-}Cy5.5}$ NCs (insulin dose 80 IU kg^{-1}, $PG_{EDA\text{-}FPBA}$ NPs 36 mg kg^{-1}) and $PG_{EDA\text{-}FPBA\text{-}Cy5.5}$ NPs ($PG_{EDA\text{-}FPBA}$ NPs 36 mg kg^{-1}) measured over 96 h in the Akita mice. d) Representative NIR images of $PG_{EDA\text{-}FPBA\text{-}Cy5.5}$ NPs (red color) in ipsilateral and contralateral inguinal LNs 1 h after SC injection (WT mice). iLiLN, ipsilateral inguinal LN; CLiLN, contralateral LN. e) Representative NIR images of Ins-$PG_{EDA\text{-}FPBA\text{-}Cy5.5}$ NCs and $Ins_{\text{-}Cy7.5}$-$PG_{EDA\text{-}FPBA\text{-}Cy5.5}$ NCs in LNs from Akita mice treated as described above. iL, ipsilateral; CL, contralateral; iLN, inguinal LN; BrLN, Brachial LN; AxLN, Axillary LN; MLN, mesenteric LN. Scale bar: 3 mm f) Representative NIR images of $Ins_{\text{-}Cy7.5}$-$PG_{EDA\text{-}FPBA\text{-}Cy5.5}$ NCs in inguinal LNs 24 h after SC injection (Akita mice). Scale bars: 3 mm. g) Representative images of the distribution of Ins-$PG_{EDA\text{-}FPBA\text{-}Cy5.5}$ NCs in iLNs 24 h after SC injection. Scale bar: 70 µm. Cell membrane (green, Wheat Germ Agglutinin-FITC); insulin (red, insulin monoclonal antibody); $PG_{EDA\text{-}FPBA\text{-}Cy5.5}$ NPs (pink, cy5.5); cell nucleus (blue, Hoechst staining). h–k) Representative STORM images of Ins-$PG_{EDA\text{-}FPBA\text{-}Cy5.5}$ NCs in plasma (24 h, h), liver (24 h, j), and kidney (24 h, k) in Akita mice and $Ins_{Cy7.5}$-$PG_{EDA\text{-}FPBA}$ NCs in plasma (24 h, i) in Akita mice. Scale bar: 500 nm and 100 nm (inset), respectively in (h); Scale bar: 6 µm and 300 nm (inset), respectively in (i); Scale bar: 2 µm and 200 nm (inset) in (j), Scale bar: 6 µm in (k). The error bars represent the mean ± SD (n = 3 per group).

are rapidly absorbed by blood capillaries, Ins-$PG_{EDA\text{-}FPBA}$ NCs or $PG_{EDA\text{-}FPBA}$ NPs are too large to cross the tight endothelial junctions in blood capillaries.[16,25] We therefore hypothesize that Ins-$PG_{EDA\text{-}FPBA}$ NCs can enter the systemic circulation through the lymphatic system as it is reported that lymphatic capillaries enable the uptake of high molecular weight biomolecules and NPs.[25] To verify this hypothesis, we examined several major lymph nodes (LNs) at different time points after SC injection of Ins-$PG_{EDA\text{-}FPBA\text{-}Cy5.5}$ NCs and control (unlabeled naked insulin), and $PG_{EDA\text{-}FPBA\text{-}Cy5.5}$ NPs, naked $Ins._{Cy7.5}$, and dual-labeled $Ins._{Cy7.5}$-$PG_{EDA\text{-}FPBA\text{-}Cy5.5}$ NCs in Akita mice and STZ-induced diabetic mice. In healthy C57BL/6 mice, the $PG_{EDA\text{-}FPBA\text{-}Cy5.5}$ NPs firstly and promptly (within 1 h) reached the ipsilateral (iL) inguinal LNs (iLNs) through the wide opening of the specialized gaps (also known as junctions, up to ≈100 nm) between lymphatic endothelial cells in the lymphatic capillaries, and subsequently migrate to contralateral iLNs (CL iLNs) via the lymphatic vessels.[26] (Figure 5d and Figure S20, Supporting Information). The lymphatic vessels form a one-way trafficking pathway for lymph and leukocytes that specifically encompass tight "zipper-like" junctions for prevention of lymph leakage during lymphatic drainage.[27] Thus, we also examined both the ipsilateral (iL) and contralateral (CL) iLNs, axillary LNs (AxLNs), brachial LNs (BrLNs), and mesenteric LNs (MLNs) 24 h after SC injection of Ins-$PG_{EDA\text{-}FPBA\text{-}Cy5.5}$ NCs or $Ins._{Cy7.5}$-$PG_{EDA\text{-}FPBA\text{-}Cy5.5}$ NCs in the Akita mice (Figure 5e) and STZ-induced diabetic mice (Figure S21, Supporting Information). $Ins._{Cy7.5}$-$PG_{EDA\text{-}FPBA\text{-}Cy5.5}$ NC was detected in the iLNs and associated lymphatic vessels 24 h post-SC injection in the Akita mice (Figure 5f) and STZ-induced diabetic mice (Figure S22, Supporting Information). A similar uptake of Ins-$PG_{EDA\text{-}FPBA\text{-}Cy5.5}$ NCs into LNs was observed in WT C57BL/6 mice (Figure S23, Supporting Information). Furthermore, the distribution of Ins-$PG_{EDA\text{-}FPBA}$ NCs into different areas of iLNs in the Akita mice was visualized using confocal microscopy imaging (Figure 5g). Super-resolution microscopy images with a nanoscale resolution, acquired from blood 24 h post-injection revealed the presence of intact circulating Ins-$PG_{EDA\text{-}FPBA}$ NCs (Figure 5h), with insulin molecules appearing still bound to the nanocarrier (Figure 5i). As the literature reports, the presence of surface hydrophilicity, and optimal particle size, and flexibility are critical for lymphatic transport. For example, the lymphatic transport of dextran chains with high flexibility is superior to that of rigid polystyrene spheres.[27b,28] The excellent lymphatic transport properties displayed by the Ins-$PG_{EDA\text{-}FPBA}$ NCs may likely be due to the intrinsic size, hydrophilicity, and flexibility of the multilobular nanosugar component (Figure S1, Supporting Information). However, further studies are required to determine whether lymphatic transport of the nanosugars (Ins-$PG_{EDA\text{-}FPBA}$ NCs) occurs via passive transport, active cell-mediated trafficking, or mixed mechanisms. Our results indicate that both the Ins-$PG_{EDA\text{-}FPBA}$ NCs and $PG_{EDA\text{-}FPBA}$ NPs navigate the lymphatic system upon injection into the SC tissue by entry into lymphatic capillaries, migrating to primary and ipsilateral LNs and subsequently entering the contralateral LNs or thoracic duct and right lymphatic trunk to access the systemic circulation and accumulate in the liver.[27b] Indeed, analysis of the fixed liver tissue by H&E staining and confocal microscopy revealed that the Ins-$PG_{EDA\text{-}FPBA\text{-}Cy5.5}$ NCs can likely cross the organ's fenestrated endothelium, which permits the passage of NPs of up to 100 nm in diameter[29] (Figure S24, Supporting Information). Ins-$PG_{EDA\text{-}FPBA\text{-}Cy5.5}$ NCs are then taken up by hepatocytes and enter the intrahepatic system of bile ducts (Figure S25, Supporting Information). STORM super-resolution analysis of the fixed liver tissues further demonstrated the presence of intact ins-$PG_{EDA\text{-}FPBA}$ NCs (Figure 5j), whereas a widespread signal was detected in the kidney (Figure 5k), confirming that Ins-$PG_{EDA\text{-}FPBA}$ NCs are amenable to degradation in vivo. The Ins-$PG_{EDA\text{-}FPBA}$ NCs were also identified in the bile and feces (Figure S26, Supporting Information), indicating that Ins-$PG_{EDA\text{-}FPBA}$ NCs enter the hepatobiliary excretion pathway.[29] These data allow us to infer that Ins-$PG_{EDA\text{-}FPBA}$ NCs entering the hepatic portal vein are taken up and processed by liver hepatocytes and finally undergo either intracellular hepatic degradation or hepatobiliary excretion via the bile duct. Notably, histology of liver tissue and the skin injection site indicated no liver damage or inflammation after administration of Ins-$PG_{EDA\text{-}FPBA}$ NCs in Akita mice (Figure S24 and S27, Supporting Information).

3. Conclusion

Innovative technologies for diabetes treatment which act like an artificial pancreas in vivo[30] are in great demand but still unattained. The clinical translation of biomaterials formulated to gain glucose responsive insulin delivery is typically hampered by long-term biocompatibility and bioavailability issues, variability in the insulin release profile and risk of hypoglycaemia. We engineered a glucose-responsive nanosugar and demonstrated its potential as a highly biocompatible glucose-responsive insulin delivery platform for diabetes treatment using two distinct insulin-deficient diabetic mouse models. We show that insulin was delivered by the engineered Ins-$PG_{EDA\text{-}FPBA}$ NCs after a single subcutaneous (SC) injection in mice, in a therapeutically relevant dose and time scale resulting in optimal blood glucose levels (below 200 mg dL^{-1}) for up to 13 h. Unlike other preclinical studies that only used type 1 diabetic mouse, rat, or large-animal (minipig) models induced by an insulin-producing β-cell-cytotoxic drug, streptozotocin (STZ),[11,14–15] we first employed a reliable spontaneously insulin-deficient type 1 diabetic Akita mouse model (C57BL/6-Ins2-Akita/J) to study the therapeutic properties of glucose-responsive materials. It was reported that the unexplained vital organs related off target toxicities of STZ may interfere with the studies conducted on the chemically induced type 1 diabetes model.[31] The mechanism of action of the engineered nanosugar for glucose control in two distinct diabetic mice models was comprehensively elucidated by combining single-molecule localization microscopy and biodistribution and pharmacokinetics studies.

Our findings suggest that a rapid glucose-responsive insulin release is mediated by Ins-$PG_{EDA\text{-}FPBA}$ NCs that are capable of promptly sensing high glucose levels and a fast in situ insulin release by a surface charge switch mechanism (**Figure 6**). Similar rapid in situ glucose triggered insulin release profile has been observed in other glucose-response biomaterials.[6,11,14–15] However, the engineered glucose responsive Ins-$PG_{EDA\text{-}FPBA}$ NCs have unique intrinsic size, hydrophilicity, biodegradability,

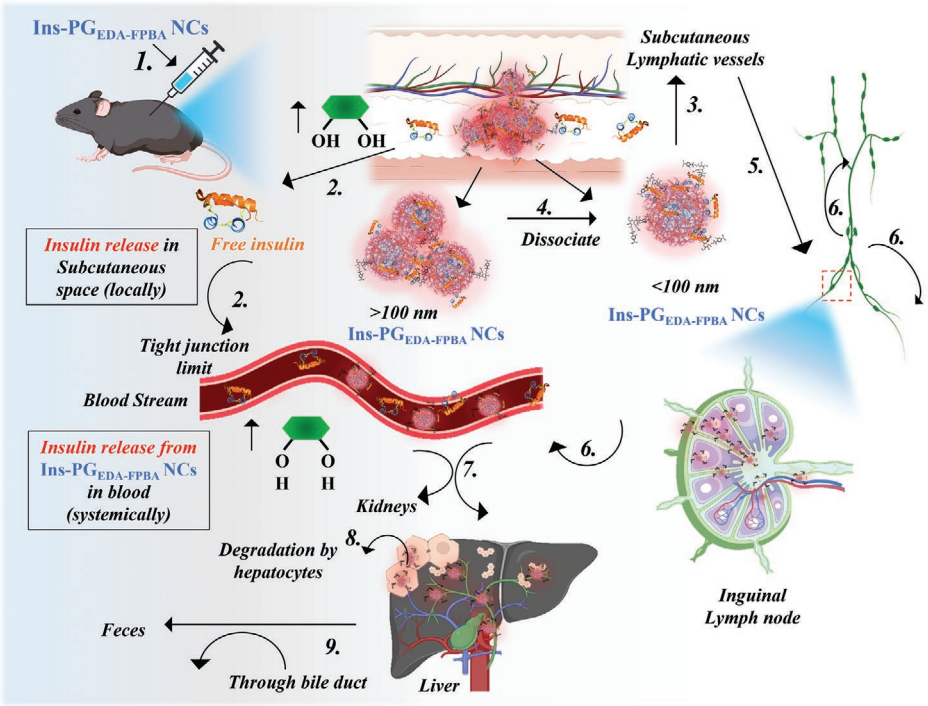

Figure 6. Mechanism of action of the engineered nanosugar for glucose control in diabetic mice. SC injection of engineered nanosugar (Ins-PG$_{EDA-FPBA}$ NCs) in diabetic mice (**1**.). Rapid local insulin release from Ins-PG$_{EDA-FPBA}$ NCs in response to a high glucose level in the SC space. The released insulin readily enters the blood stream (**2**.). The small NCs (50–100 nm) travel through the interstitial space and directly enter lymphatic vessels (**3**.), as lymphatic endothelial cells gaps are opened to ≈100 nm, and rapidly migrate to ipsilateral LNs (for example, iLNs) within 1 h of injection (**5**.), and then distribute to contralateral LNs (**6**.) or enter the thoracic duct to finally access the blood stream (**6**.) for systemic distribution and release of insulin in the blood. This process is slow but constantly occurs from the SC injection site to the lymphatic system and then blood circulation (steps **3**., **5**., **6**.). Concurrently, the large NCs (100–300 nm) are retained within the SC space because of their large size and slowly dissociate into smaller NCs and release the embedded insulin in a controlled and glucose-responsive fashion (**4**.). The circulating Ins-PG$_{EDA-FPBA}$ NCs are not filtered by the kidneys but sequestrated in the liver where they are degraded by hepatocytes (**8**.) or enter the hepatobiliary excretion pathway via the liver–bile–feces axis (**9**.).

and tunable morphology. We provided evidence that the small NCs (50–100 nm) can readily and passively diffuse through the extracellular matrix network under the skin to access the LNs and navigate the lymphatic system toward the blood stream. In circulation, intact small NCs respond rapidly and directly to dynamic changes in blood glucose to regulate insulin release (Figures 2e and 5h,i). Interestingly, large Ins-PG$_{EDA-FPBA}$ NCs (100–300 nm) remain confined to the SC tissue and perform as glucose-responsive reservoirs that promptly and continuously disassemble upon glucose challenge and release insulin through the blood capillaries (Figure 6). The release of insulin is controlled by the equilibrium between the complex and the unbound PG$_{EDA-FPBA}$ NPs and insulin species. The equilibrium is shifted toward the unbound forms when the charge density on PG$_{EDA-FPBA}$ NPs is reduced upon glucose binding, because the electrostatic interactions are weakened. In addition, in the SC tissue the free/unbound insulin is depleted due to the diffusion into the blood capillaries, hence free insulin molecules will be released to establish the equilibrium condition. Large NCs in situ and small NCs in circulation may enable the sustained release of insulin over 13 h, as per our observations. The circulating NCs are sequestrated in the liver where they are degraded by hepatocytes or enter the hepatobiliary excretion pathway via the liver–bile–faeces axis. Overall, the highly biocompatible PG$_{EDA-FPBA}$ NPs provide an excellent platform for the assembly and transport of insulin molecules by several mechanisms, enabling control over the pharmacokinetic properties of the released insulin. In addition, the nanocomplexation process imparts storage stability to the formulation and prevents the aggregation of insulin in the SC tissue, thereby improving insulin bioavailability. Our technology provides a strong framework for the formulation of a glucose-responsive insulin delivery system for potential clinical translation. Although the engineered nanosugar showed efficacy in two distinct diabetic mouse models, to advance this formulation toward clinical studies, it is essential to scale up the manufacturing process, investigate long-term storage stability, and evaluate the safety and efficacy of the formulation in large-animal and primate models. Based on our results, the engineered glucose-responsive nanosugars emerges as a promising platform that can potentially meet these requirements. The morphology of the nanocomplexes can be tailored to program the rate of insulin release and further prolong the insulin bioavailability. This study therefore paves the way for future treatment of diabetes with a natural, and highly biocompatible nanosugar sourced from sweet corn that mitigates the risks of hyperglycemia and hypoglycemia. In addition, our strategy could be extended to the delivery of other therapeutic peptides and proteins (i.e glucagon-like protein 1 (GLP1) and GLP1 agonists)

4. Experimental Section

Synthesis of PG_{EDA} NPs: PG (200 mg, equivalent to 1.2 mmol of glucose monomers) was dissolved in acetic buffer (5 mL, 0.6 M, pH 5.5) with stirring. To this solution, sodium periodate (42 mg, 0.24 mmol) was added in the dark for oxidation of the 1,2 diols. After 2 h, EDA (72 mg, 1.2 mmol) was added followed by the addition of sodium cyanoborohydride (10 eq.), and the mixture was stirred overnight. The product (PG_{EDA} NPs) was purified by dialysis (molecular weight cutoff (MWCO) 14 kDa) against Milli-Q water for 3 days (the medium was changed 6 times) and freeze dried. The yield of the reaction was ≈90%.

Synthesis of $PG_{EDA\text{-}FPBA}$ NPs: FPBA (40 mL; 110 mg, 0.6 mmol) was added to a mixture of *N*-hydroxysuccinimide (NHS; 140 mg, 1.2 mmol) and *N*-(3-dimethylaminopropyl)-*N'*-ethylcarbodiimide hydrochloride (EDC•HCl; 120 mg, 0.6 mmol) and stirred for 30 min. Next, PG_{EDA} NPs (100 mg) were added to the reaction mixture and stirred overnight in dark. The product ($PG_{EDA\text{-}FPBA}$ NPs) was purified by dialysis (MWCO cutoff 14 kDa) against NaCl (0.1 M) for 1 day and Milli-Q water for 3 days (6 times changed) and freeze dried. The yield of the reaction was ≈87%. The NPs were characterized by ^{1}H-NMR spectroscopy, absorption spectroscopy, and DLS.

Labeling of Insulin and $PG_{EDA\text{-}FPBA}$ NPs for STORM and FCS Analyses: $PG_{EDA\text{-}FPBA}$ NPs (5 mg mL^{-1}) were dissolved in sodium bicarbonate buffer pH = 8 (100 mM) and mixed with AF488-NHS, AF647-NHS, Cy5.5, or Cy7.5 (20 µL, 1 mg mL^{-1}) dye. The mixture was stirred overnight, and excess dye was removed using NAP-10 column and freeze dried. Similarly, for studying the colocalization of insulin and $PG_{EDA\text{-}FPBA}$ NPs with STORM, insulin (2 mg mL^{-1}) in $NaHCO_3$ (100 mM) was incubated overnight with AF488-NHS (35 µL, 1 mg mL^{-1}) and AF647-NHS (8 µL, 1 mg mL^{-1}) dyes and purified via dialysis against water (dialysis tubing size was 10 kDa). $PG_{EDA\text{-}FPBA}$ NPs (1.5 mg mL^{-1}) were likewise incubated with AF647-NHS (12 µL) and AF555-NHS (20 µL) dyes, and the mixture was stirred overnight, and excess dye was removed using NAP-10 column and freeze dried.

Characterization of Engineered NPs and NCs by NMR Spectroscopy and UV–Vis Spectroscopy: ^{1}H-NMR spectra of PG NPs, PG_{EDA} NPs, and $PG_{EDA\text{-}FPBA}$ NPs were recorded on a 600 MHz Bruker Avance III at 40 °C in H_2O and 10% D_2O using the sequence (zgesgp) and the following parameters: 128 scans, 2 s relaxation delay, and spectral width of 9.6 kHz. ^{1}H-NMR spectra of insulin, Ins-$PG_{EDA\text{-}FPBA}$ NCs, Ins-PG_{EDA} NCs, and Ins-PG NCs were recorded on a 700 MHz Bruker Avance IIIHD at 25 °C in H_2O and 10% D_2O using the sequence (zgesgp) and the following parameters: 64 scans, 2 s relaxation delay, and spectral width of 11.2 kHz. The spectra were processed using Topspin 4.1.4, and ^{1}H chemical shifts were referenced to d_4-trimethylsilylpropanoate at 0 ppm. UV–vis spectroscopy was performed using SPECORD 250 PLUS. A 1 cm quartz cuvette was used to analyze a solution of $PG_{EDA\text{-}FPBA}$ NPs (1 mg ml^{-1}, pH 7) and a calibration curve for FPBA was generated. The scattering of the PG NPs at the same concentration was subtracted from the spectra.

Degradation of $PG_{EDA\text{-}FPBA}$ NPs by α-Amylase and β-Amylase: The rate of degradation of PG NPs and $PG_{EDA\text{-}FPBA}$ NPs by α-amylase and *β-amylase* was determined using the Somogyi–Nelson assay. The PG or $PG_{EDA\text{-}FPBA}$ NPs (200 µL, 1 mg mL^{-1}) were dissolved in 10 mM PBS (pH = 7.4) and incubated for 1, 2, and 3 h with enzyme solutions, where the final concentration of the enzyme was 1 U mL^{-1}. Following incubation, the samples were analyzed using the Somogyi–Nelson assay. For the assay, copper-carbonate-tartrate reagent, which is composed of stock I (sodium potassium tartrate tetrahydrate (1.2 g), sodium carbonate (2.4 g), sodium bicarbonate (1.6 g), and sodium sulfate (14.4 g) in 80 mL of Milli-Q water) and stock II (copper sulfate pentahydrate (0.4 g) and sodium sulfate (3.) dissolved in 20 mL of Milli-Q water), was prepared. The working reagent was then prepared by mixing 4 parts of stock I with one part of stock II. The arsenomolybate color reagent was prepared by dissolving ammonium molybdate (2.5 g) in water which was then mixed with concentrated sulfuric acid (2.1 mL). This solution was mixed with a solution of sodium arsenate dibasic pentahydrate (0.3 g in 2.5 mL of Milli-Q water). Aliquots (45 µL) of PG or $PG_{EDA\text{-}FPBA}$ NPs solution, in triplicate, before and after treatment with α-amylase were added to a 96-well microplate (Costar 3596, Corning, MA, USA). The working reagent (45 µL) was added and the plate was covered in Al foil and heated at 90 °C for 20 min. The plate was cooled to room temperature and arsenomolybate color reagent (45 µL) was added to each well, and after 15–20 min, the absorbance was recorded at 600 nm using an Infinite M200 microplate reader (Tecan, Switzerland).

Cell Viability: Cell viability was measured using an alamarBlue assay. 3T3 Fibroblasts and raw cells were plated on a 96-well plate at a seeding density of 7000 cells per well in Dulbecco's modified Eagle medium (DMEM; 100 µL) supplemented with 10% fetal bovine serum. After 24 h, cells were incubated with different concentrations of $PG_{EDA\text{-}FPBA}$ NPs for 96 h. Cell viability was estimated after incubating the cells with alamarBlue reagent for 2 h using an Infinite M200 microplate reader.

Complexation between Insulin and $PG_{EDA\text{-}FPBA}$ NPs to Form Ins-$PG_{EDA\text{-}FPBA}$ NCs: Both $PG_{EDA\text{-}FPBA}$ NPs (20 mg mL^{-1} in Milli-Q water) and insulin were dissolved (1 mg, 28.8 U, in 0.01 N HCl). The complexes were then prepared with different weight-to-weight (w/w) ratio of insulin and $PG_{EDA\text{-}FPBA}$ NPs in Milli-Q water (pH 6) and PBS (50 mM, pH 7). Then, the complexes were purified using a 100 kDa spin column at 10000 rpm for 5 min, and the supernatant was analyzed by fluorescence spectroscopy (emission at 310 nm at excitation wavelength 275 nm) and high-performance liquid chromatography to estimate the amount of loading. The size and charge of the complexes were measured by DLS and electrophoretic mobility, respectively, and the morphology was studied by STORM. The complexes were also prepared in the presence of PBS (20 mM, pH ≈7), where $PG_{EDA\text{-}FPBA}$ NPs were dissolved in PBS and the pH of the insulin solution was gradually increased to ≈6.5.

For the in vivo studies, Ins-$PG_{EDA\text{-}FPBA}$ NCs were prepared as follows: in the presence of PBS (20 mM, pH ≈7), $PG_{EDA\text{-}FPBA}$ NPs (6 mg mL^{-1}) were complexed with insulin at an insulin-to-$PG_{EDA\text{-}FPBA}$ NPs weight ratio of 1:13 overnight at 4 °C.

Characterization of Ins-$PG_{EDA\text{-}FPBA}$ NCs by STORM, FCS, and TEM: For STORM analysis, FITC-Ins-$PG_{EDA\text{-}FPBA}$ NCs were prepared as described above at varying Insulin-to-$PG_{EDA\text{-}FPBA}$ NPs weight ratios of 1:0, 1:1.5, 1:3.5, 1:10, 1:13. Ins-$_{FITC}$ -$PG_{EDA\text{-}FPBA}$ NCs were deposited on a glass slide, and after 30 min of incubation at 25 °C, unbound molecules and NPs were washed away with freshly prepared, standard imaging buffer with cysteamine (MEA). STORM images were acquired on a Nikon N-STORM system equipped with a Nikon 100 × 1.4 NA oil immersion objective. The focus and total internal reflection fluorescence imaging angle were adjusted to obtain a high signal-to-noise ratio. Lasers (647, 561, and 488 nm) were used for the excitation of the fluorophores. All time lapses were recorded within a 256 × 256 pixels region using an EMCCD camera. For each image, 4000 frames were acquired sequentially using full laser power. STORM images were first processed with the STORM module of the NIS Elements Nikon software, where drift correction was performed, and a list of particle localizations was obtained by Gaussian fitting of the fluorescence spots of blinking dyes. Blinking events that were detected in ≤5 consecutive frames were counted as single molecules, whereas events detected in >5 consecutive frames were discarded (max trace length 5). The list of localizations was exported as a .txt file and analyzed using an in-house-built clustering analysis script on Spyder (Anaconda3 software), where the localizations were clustered using a kernel density estimation with a bandwidth of 50 nm. An ellipse was fitted to the obtained clusters with a minimum of 10 localizations and a maximum elongation factor of 1.5 (ratio of long and short axes of the ellipse). Then, the circles containing 90% of detected spots in the cluster were fitted to determine the NP size distribution and number of localizations. For the multicolour STORM analysis, insulin was dual labeled with AF488/AF647 (green) and the $PG_{EDA\text{-}FPBA}$ NPs were dual labeled with AF555/AF647 (red). FCS experiments on AF647 $PG_{EDA\text{-}FPBA}$ NPs incubated with enzymes were performed on a Nikon A1R confocal microscope combined with a MicroTime PicoQuant system with 40 × /1.1 NA water immersion objective and a 647 nm laser for illumination. The confocal volume (Veff) was calibrated by the measurements of AF 647 dye with the known DAF647 = 3.3 ± 0.1 × 10^{-6} cm^2 s^{-1} at the beginning of each experiment. The measurements were carried

out for 30 s and repeated at least 20 times in various positions. The generated autocorrelation function (ACF) curves were analysed using the SymPhoTime 64 software. For TEM imaging, a drop (10 µL) of a sample dispersion (10 mg mL^{-1}) was deposited on a copper grid for 10 min. Excess sample was then removed and the grid was washed with Milli-Q water twice. Subsequently, uranyl acetate (10 µL) was added to the grid for 1 min and the grid was washed twice with water. The grid was then air dried and imaged on a JEOL JEM-1010 transmission electron microscope. Cryo-TEM images were obtained using a TECNAI F30 microscope equipped with a high-angle annular dark-field scanning transmission electron microscopy detector, a Gatan quantum 965 energy filter, and an upper CETA 4k × 4k CMOS camera.

Circular Dichroism (CD) Spectroscopy: Ins-$PG_{EDA\text{-}FPBA}$ NCs (ratio 1:13) and naked insulin samples were prepared as described above and then diluted 8 times with Milli-Q water. Each sample was split into two aliquots: the first aliquot was treated at 60 °C for 1 h with shaking at 300 rpm and the second aliquot was kept at RT for 1 h. CD spectra were acquired on a Chirascan spectropolarimeter (Applied Photophysics Ltd., UK) between 190 and 260 nm using a 0.1 mm path length cylindrical quartz cell (Starna Scientific Ltd, Hainault, UK). Spectra were acquired with 0.5 nm data intervals, 1 s integration time, and 3 scans accumulation. Signal was recorded as millidegrees at 25 °C. Spectra were zeroed at 260 nm, the background from the solvent or $PG_{EDA\text{-}FPBA}$ NPs was subtracted, and normalized to give units of mean-residue ellipticity (MRE) according to $[\theta]\text{MRE} = \theta/(c \times l \times \text{Nr})$, where θ is the recorded ellipticity (mdeg), c is the peptide concentration (dmol L^{-1}), l is the cell path length (cm), and Nr is the number of residues.

Effect of Glucose on $PG_{EDA\text{-}FPBA}$ NPs: The effect of glucose concentration on the ζ-potential of $PG_{EDA\text{-}FPBA}$ NPs (10 mg mL^{-1}) was determined after the addition of different amounts of glucose (100 and 400 mg dL^{-1}) below and above the pK_a of FPBA. The binding of glucose to $PG_{EDA\text{-}FPBA}$ NPs was quantified as follows. Glucose (100 or 400 mg dL^{-1}) was added to 300 µL of 8 mg mL^{-1} PG_{EDA} NP or $PG_{EDA\text{-}FPBA}$ NP solution in PBS (100 mM, pH 7.4), and the mixture was incubated at 37 °C. After various time points, the supernatant was collected using a spin column and the glucose concentration was estimated using an Accu-Chek Performa glucose monitor.

In Vitro Insulin-Release Study: Briefly, the PG_{EDA} and $PG_{EDA\text{-}FPBA}$ NCs with 0.3 mg insulin were incubated with PBS and with different concentrations of glucose (100 and 400 mg dL^{-1}) at pH 7.4 in centrifuge tubes. The centrifuge tubes were incubated at 37 °C and stirred at 500 rpm. The supernatant was then recovered after various time points using a 100 kDa spin column at 10 000 rpm for 5 min and analyzed by fluorescence spectroscopy (emission at 310 nm at excitation wavelength 275 nm) to estimate the amount of loading. When FITC-conjugated insulin was used, the fluorescence emission was recorded at 515 nm at an excitation wavelength of 480 nm.

In Vitro Assessment of Insulin Bioactivity of Ins-$PG_{EDA\text{-}FPBA}$ NCs: HepG2 cells (0.5×10^6; human liver hepatocellular carcinoma, American Type Culture Collection, HB-8065) were seeded over 48 h with 10% FCS/DMEM (1 × penicillin–streptomycin) and starved in serum-free DMEM media overnight. Insulin (equivalent concentration of 100 nM) was then loaded into the $PG_{EDA\text{-}FPBA}$ NPs at an Insulin-to-$PG_{EDA\text{-}FPBA}$ NPs ratio of 1:13. An aliquot (2 µL) of each sample was added to the HepG2 cells and incubated for 15 min. The medium was then discarded, and the cells were washed with PBS twice, and RIPA buffer with a phospho-inhibitor cocktail and protease inhibitor cocktail was added for cell lysis. The supernatant was collected after centrifugation at 16 000*g* for 30 min, and the protein amount was quantified using the BCA kit before the supernatant was added to 6 × sodium dodecyl sulfate sample buffer and heated at 95 °C for 10 min. For immunoblotting, each cell lysate (60 µg) was loaded into 12% acrylamide gel for electrophoresis, as previously described.[32] Transferred membrane were probed with primary antibodies (rabbit p-AKT Ser473, Pan-AKT, 1:1000 dilution). Incubation transferred membrane with secondary antibody (goat anti-rabbit HRP, 1:3000 dilution). Membranes were washed thrice with PBS and the chemiluminescent Western Blot reagent was added (Thermo Fisher Scientific). Images were obtained using a ChemiDoc machine (BioRad) and quantified using Image Lab 6.1 (BioRad).

Ex Vivo Plasma Insulin-Release Study: Blood samples were collected from healthy donors, with informed consent, at the Australian Centre for Blood Diseases. PPP was obtained after centrifugation at 2000 g for 10 min twice. Samples (25 µL) were prepared that were either normal PPP glucose (100 mg dL^{-1}) or diabetic PPP glucose (600 mg dL^{-1}, additional glucose was added to normal PPP). All samples had an equivalent insulin concentration of 1.33 IU mL^{-1} and were incubated at 37 °C while shaking at 500 rpm. The supernatant was then recovered after various time points using a 100 kDa spin column at 10000 g for 5 min and analyzed for the free insulin amount via ELISA (ALPCO 80-INSMSU-E01 kit). The supernatant was diluted 3000 × using a Zero standard solution from the ELISA kit. Briefly, aliquots (5 µL) of each of the standard curve samples, insulin controls, and final diluted samples were loaded into a 96-well microplate. A working conjugate buffer (75 µL) was added, and the microplate was sealed and placed on an Eppendorf Thermomixer machine for 2 h and mixed at 800 rpm. Wells were washed 6 times with working strength wash buffer (350 µL) before tetramethylbenzidine (TMB) Substrate (100 µL) was added. The microplate was incubated for a further 30 min at room temperature while shaking at 800 rpm. The Stop Solution (100 µL) was added to each well and the absorbance was measured using a FLUOstar OPTIMA machine at 450 nm.

In Vivo Blood Glucose Regulation Studies in Akita and STZ-Induced Type-1 Diabetic Mice Models: In vivo studies were conducted using 8–12-week-old heterozygous Akita type 1 diabetic male mice (C57BL/6-Ins2-Akita/J) purchased from the Alfred Research Alliance Precinct Animal Centre (Australia). All animal procedures were approved by the Alfred Research Alliance Animal Ethics Committees (ARAAEC), Monash University (AEC number E/1695/2016/M and E/P8220/2022). STZ induction was conducted by continuous intraperitoneal injection of STZ at low dose (55 mg kg^{-1}) over 5 days, and blood glucose was monitored over 4–5 weeks. The mice were considered diabetic when the BGL was over 25 mg dL^{-1}. Akita mice (n = 5) and STZ-induced diabetic mice (n = 3–4) were distributed into groups treated with naked insulin (insulin dose 16 IU kg^{-1}) and NCs (e.g., insulin dose 80 IU kg^{-1}). The blood glucose was monitored before and after treatment until the blood glucose returned to initial levels. The blood samples were taken from the tail tip and plasma glucose concentration was measured by a glucose meter (ACCU-CHEK). Blood samples (2.5 µL) of the Akita mice (n = 3) and STZ-induced diabetic mice (n = 3) treated with native insulin (insulin dose 16 IU kg^{-1}) and NCs (insulin dose 80 IU kg^{-1}) were extracted and transferred into Eppendorf tubes and mixed with 2.5 µL 10% sodium citrate (3.2%) PBS solution. The obtained blood was centrifuged (2000 g, 15mins, twice) and the plasma was stored at –20 °C until measurement. The plasma insulin level was quantified via ELISA.

IPGTT in Akita and STZ-Induced Type 1 Diabetic Mice: Akita (n = 3–4) and STZ-induced type 1 diabetic mice (n = 3–4) were randomly assigned to be treated with insulin NCs (80 IU kg^{-1}) and naked insulin (16 IU kg^{-1}). At 4 h post-treatment, the Akita and STZ-induced diabetic mice were intraperitoneally injected with glucose (1.5 g kg^{-1}). The blood samples were taken from the tail tip and the plasma glucose concentration was measured by a glucose meter (ACCU-CHEK).

Intraperitoneal Glucose Injection Induced Insulin Release Study in Akita and STZ-Induced Type 1 Diabetic Mice: Akita (n = 3–4) and STZ-induced type 1 diabetic mice (n = 3) were randomly assigned to be treated with various insulin NCs (insulin dose 80 IU kg^{-1}). At 4 h post-treatment, the Akita mice were intraperitoneally injected with glucose (1.5 g kg^{-1}). Blood samples (2.5 µL) were extracted and transferred into Eppendorf tubes and mixed with 2.5 µL 10% sodium citrate (3.2%) PBS solution. The obtained blood was centrifuged, and the plasma was stored at –20 °C until measurement. The plasma insulin level was quantified via ELISA.

Biodistribution Studies in Akita, STZ-Induced Diabetic, and WT C57BL/6 Mice: Mice were housed on a 12 h light/dark cycle with ad libitum access to food and water. Biodistribution studies were conducted using Akita male mice (8–12 weeks old), STZ-induced C57Bl/6 male mice (12–13 weeks old), and C57BL/6 male mice (8–12 weeks old) bred in house. All animal experiments were approved by the ARAAEC Monash

University (AEC number Akita mice E/1695/2016/M and C57Bl/6 mice E/1625/2016/M). To evaluate the biodistribution of Ins-$PG_{EDA\text{-}FPBA}$ NCs and $PG_{EDA\text{-}FPBA}$ NPs, the mice were subcutaneously administered Ins-$PG_{EDA\text{-}FPBA\text{-}Cy5.5}$ NCs (insulin dose 80 IU kg^{-1}) and naked insulin (control, insulin dose 16 IU kg^{-1}), $Ins_{\text{-}Cy7.5}$-$PG_{EDA\text{-}FPBA\text{-}Cy5.5}$ NCs (insulin dose 80 IU kg^{-1}), naked $Ins_{\text{-}Cy7.5}$ (insulin dose 16 IU kg^{-1}), or $PG_{EDA\text{-}FPBA\text{-}Cy5.5}$ NPs (36 mg kg^{-1}) (Akita mice ($n = 3$) and STZ-induced mice ($n = 3$)). In WT C57BL/6 mice, $PG_{EDA\text{-}FPBA\text{-}Cy5.5}$ NPs (36 mg kg^{-1}), Ins-$PG_{EDA\text{-}FPBA\text{-}Cy5.5}$ NCs (insulin dose 24 IU kg^{-1}, NPs 36 mg kg^{-1}), Ins-$PG_{EDA\text{-}FPBA\text{-}Cy5.5}$ NCs (insulin dose 12 IU kg^{-1}, NPs 36 mg kg^{-1}), or Ins-$PG_{EDA\text{-}FPBA\text{-}Cy5.5}$ NCs (insulin dose 8 IU kg^{-1}, NPs 36 mg kg^{-1}) were administrated subcutaneously. Blood samples were then collected from the mouse tail and blood withdrawn (2.5 µL) using a pipette at the indicated time points post-injection. Collected blood was diluted in 10% sodium citrate (3.2%) PBS solution (total volume 50 µL) and those diluted blood samples (50 µL) were measured on an Odyssey CLx scanner (LI-COR Biosciences, NE, USA), with the fluorescence detected using the 800 nm (Cy7.5 dye) or 700 nm (Cy5.5) channel, accordingly.

At indicated time points, the mice were euthanized by an overdose intraperitoneal injection of ketamine (300 mg kg^{-1}) and xylazine (30 mg kg^{-1}) and subsequently subjected to transcardial perfusion with PBS (20 mL) before the brain, heart, lung, liver, spleen, kidney, muscle, and skin were harvested. The organs were briefly washed and stored in PBS at 4 °C and in the dark until fluorescence imaging was performed. The scans were recorded on an Odyssey CLx scanner, with the fluorescence detected using the 800 nm (Cy7.5 dye) or 700 nm (Cy5.5 dye) channel. The mean fluorescence intensity value (a.u.) was determined for each sample, as well as the total fluorescence of each injected dose, calculated from a standard curve of stock volume. The percentage of the remaining material for blood clearance, and the percentage of injected dose per gram tissue for biodistribution, were calculated.[33]

Immunohistochemistry and Immunofluorescence: Tissues were fixed in 10% neutral buffered formalin (NBF), paraffin embedded, sectioned at 4 microns, and float sections into superfrost slides. One series was subjected to H&E staining, and an Olympus BX51 fluorescence microscope was used to image the H&E-stained tissue slides. The waxed tissue slides were placed on a heating block at 60 °C for 2 h and then dewaxed with incubation with xylene (5 min, 3 times), 100% ethanol (20 dips, 3 times), and PBS (5 min, 2 times). Antigen retrieval was achieved via incubation of tissue slides with sodium citrate buffer at 90 °C for 20 min with 30 min cooling, followed by PBS washes (5 min, 2 times). Permeabilization was performed with 0.5% Triton X/PBS for 30 min at room temperature. Tissue slides were blocked with 5% serum at room temperature for 1 h. Tissue slides were incubated with primary antibody (Insulin, mouse monoclonal Antibody, eBioscience) and Wheat Germ Agglutinin Alexa Fluor 488 conjugate (WGA-AF488, Thermo Fisher Scientific for plasma membrane staining) overnight at 4 °C and washed with PBS three times, and then incubated with secondary antibody (Donkey anti-mouse AF568, Thermo Fisher Scientific) for one hour at RT and Hoechst staining at RT for 15 min. Confocal microscopy was conducted on a Nikon A1 microscope, sequentially acquiring using Plan Fluor 20 × MImm NA 0.75 objective (FITC was used for plasma membrane staining, AF568 was used for insulin staining, and channel 647 nm was used for Cy5.5 dye ($PG_{EDA\text{-}FPBA}$ NPs), Hoechst was used for nuclear staining).

Statistical Analysis: One-way analysis of variance (ANOVA) with Tukey post-hoc tests and two-way ANOVA were used to carry out multiple comparisons (Prism version 9.3.0).

Supporting Information

Supporting Information is available from the Wiley Online Library or from the author.

Acknowledgements

R.X. and S.K.B. contributed equally to this work. This work was supported by the National Health and Medical Research Council of Australia (Ideas Grant to C.E.H. and F.Cavalieri GNT1181440, Senior Research Fellowship to C.E.H. GNT1154270, Senior Principal Research Fellowship to F. Caruso GNT1135806). F. Cavalieri acknowledges the award of an RMIT Vice Chancellor Senior Research Fellowship. R.X. was supported by a Monash University Senior Postdoctoral Fellowship. This work received funding from the European Union Horizon 2020 Research and Innovation Program under the H2020 Marie Skłodowska-Curie Actions grant agreement no. 872233 ("PEPSAMATE"). The authors thank Margaret Hibbs and Evelyn Tsantikos for advice on the lymphatic system. The authors thank Monash University's Micro-Imaging Platform (Stephen Cody), AMREP Flow Cytometry Core Facility (Eva Orlowski-Oliver) and Histology Platform (Camilla Cohen). This work was performed in part at the Materials Characterization and Fabrication Platform (MCFP) and Bio21 Ian Holmes imaging Center at The University of Melbourne.

Open access publishing facilitated by RMIT University, as part of the Wiley - RMIT University agreement via the Council of Australian University Librarians

Conflict of Interest

The authors declare no conflict of interest.

Data Availability Statement

The data that support the findings of this study are available from the corresponding author upon reasonable request.

Keywords

Akita mice, glucose responsive insulin delivery, hepatobiliary excretion, phytoglycogen nanoparticles, super-resolution microscopy, type 1 diabetes

Received: November 9, 2022
Revised: January 11, 2023
Published online:

[1] a) O. Veiseh, B. C. Tang, K. A. Whitehead, D. G. Anderson, R. Langer, *Nat. Rev. Drug Discovery* **2015**, *14*, 45; b) P. Saeedi, I. Petersohn, P. Salpea, B. Malanda, S. Karuranga, N. Unwin, S. Colagiuri, L. Guariguata, A. A. Motala, K. Ogurtsova, J. E. Shaw, D. Bright, R. Williams, *Diabetes Res. Clin. Pract.* **2019**, *157*, 107843.

[2] B. Silver, K. Ramaiya, S. B. Andrew, O. Fredrick, S. Bajaj, S. Kalra, B. M. Charlotte, K. Claudine, A. Makhoba, *Diabetes Ther.* **2018**, *9*, 449.

[3] a) G. P. Carino, J. S. Jacob, E. Mathiowitz, *J. Controlled Release* **2000**, *65*, 261; b) K. Buzási, Z. Sápi, G. Jermendy, *Diabetes Res. Clin. Pract.* **2011**, *94*, e34; c) E. Chantelau, M. Spraul, I. Mühlhauser, R. Gause, M. Berger, *Diabetologia* **1989**, *32*, 421; d) M. C. Flynn, M. J. Kraakman, C. Tikellis, M. K. S. Lee, N. M. J. Hanssen, H. L. Kammoun, R. J. Pickering, D. Dragoljevic, A. Al-Sharea, T. J. Barrett, F. Hortle, F. L. Byrne, E. Olzomer, D. A. McCarthy, C. G. Schalkwijk, J. M. Forbes, K. Hoehn, L. Makowski, G. I. Lancaster, A. El-Osta, E. A. Fisher, I. J. Goldberg, M. E. Cooper, P. R. Nagareddy, M. C. Thomas, A. J. Murphy, *Circ. Res.* **2020**, *127*, 877; e) S. Saito, Y. Teshima, A. Fukui, H. Kondo, S. Nishio, M. Nakagawa, T. Saikawa, N. Takahashi, *Cardiovasc. Res.* **2014**, *104*, 5.

[4] M. J. Mitchell, M. M. Billingsley, R. M. Haley, M. E. Wechsler, N. A. Peppas, R. Langer, *Nat. Rev. Drug Discovery* **2021**, *20*, 101.

[5] Z. Gu, T. T. Dang, M. Ma, B. C. Tang, H. Cheng, S. Jiang, Y. Dong, Y. Zhang, D. G. Anderson, *ACS Nano* **2013**, *7*, 6758.
[6] L. R. Volpatti, M. A. Matranga, A. B. Cortinas, D. Delcassian, K. B. Daniel, R. Langer, D. G. Anderson, *ACS Nano* **2020**, *14*, 488.
[7] R. Yin, J. Han, J. Zhang, J. Nie, *Colloids Surf., B* **2010**, *76*, 483.
[8] J.-Z. Wu, G. R. Williams, H.-Y. Li, D.-X. Wang, S.-D. Li, L.-M. Zhu, *Drug Delivery* **2017**, *24*, 1513.
[9] C. Li, F. Huang, Y. Liu, J. Lv, G. Wu, Y. Liu, R. Ma, Y. An, L. Shi, *Langmuir* **2018**, *34*, 12116.
[10] Z. Y. Yu JC, J. Q. Wang, D. Wen, A. R. Kahkoska, J. B. Buse, Z. Gu, *Nano Res.* **2019**, *12*, 1539.
[11] J. Yu, J. Wang, Y. Zhang, G. Chen, W. Mao, Y. Ye, A. R. Kahkoska, J. B. Buse, R. Langer, Z. Gu, *Nat. Biomed. Eng.* **2020**, *4*, 499.
[12] C. Wang, Y. Ye, W. Sun, J. Yu, J. Wang, D. S. Lawrence, J. B. Buse, Z. Gu, *Adv. Mater.* **2017**, *29*, 1606617.
[13] D. H.-C. Chou, M. J. Webber, B. C. Tang, A. B. Lin, L. S. Thapa, D. Deng, J. V. Truong, A. B. Cortinas, R. Langer, D. G. Anderson, *Proc. Natl. Acad. Sci. U. S. A.* **2015**, *112*, 2401.
[14] J. Wang, J. Yu, Y. Zhang, X. Zhang, A. R. Kahkoska, G. Chen, Z. Wang, W. Sun, L. Cai, Z. Chen, C. Qian, Q. Shen, A. Khademhosseini, J. B. Buse, Z. Gu, *Sci. Adv.* **2019**, *5*, eaaw4357.
[15] J. Wang, Z. Wang, G. Chen, Y. Wang, T. Ci, H. Li, X. Liu, D. Zhou, A. R. Kahkoska, Z. Zhou, H. Meng, J. B. Buse, Z. Gu, *ACS Nano* **2021**, *15*, 4294.
[16] A. K. J. Gradel, T. Porsgaard, J. Lykkesfeldt, T. Seested, S. Gram-Nielsen, N. R. Kristensen, H. H. F. Refsgaard, *J Diabetes Res* **2018**, *2018*, 1205121.
[17] Q. A. Besford, F. Cavalieri, F. Caruso, *Adv. Mater.* **2020**, *32*, 1904625.
[18] M. Bertoldo, G. Zampano, L. Suffner, E. Liberati, F. Ciardelli, *Polym. Chem.* **2013**, *4*, 653.
[19] X. Wu, Z. Li, X.-X. Chen, J. S. Fossey, T. D. James, Y.-B. Jiang, *Chem. Soc. Rev.* **2013**, *42*, 8032.
[20] a) A. Matsumoto, T. Ishii, J. Nishida, H. Matsumoto, K. Kataoka, Y. Miyahara, *Angew. Chem., Int. Ed.* **2012**, *51*, 2124; b) Y. Shao, A. H.-M. Lin, *Food Chem.* **2018**, *240*, 898.
[21] C. Prost-Squarcioni, *Med. Sci. (Paris)* **2006**, *22*, 131.
[22] B. Kaufmann, P. Boulle, F. Berthou, M. Fournier, D. Beran, I. Ciglenecki, M. Townsend, G. Schmidt, M. Shah, S. Cristofani, P. Cavailler, M. Foti, L. Scapozza, *PLoS One* **2021**, *16*, e0245372.
[23] M. Yoshioka, T. Kayo, T. Ikeda, A. Koizuni, *Diabetes* **1997**, *46*, 887.
[24] H. A. Toque, K. P. Nunes, L. Yao, Z. Xu, D. Kondrikov, Y. Su, R. C. Webb, R. B. Caldwell, R. W. Caldwell, *PLoS One* **2013**, *8*, e72277.
[25] S. Cai, Q. Yang, T. R. Bagby, M. L. Forrest, *Adv. Drug Delivery Rev.* **2011**, *63*, 901.
[26] S. Qi, X. Wang, K. Chang, W. Shen, G. Yu, J. Du, *J. Nanobiotechnology* **2022**, *20*, 24.
[27] a) K. Alitalo, *Nat. Med.* **2011**, *17*, 1371; b) J. McCright, R. Naiknavare, J. Yarmovsky, K. Maisel, *Front. Pharmacol.* **2022**, *13*, 887402.
[28] N. A. Rohner, S. N. Thomas, *ACS Biomater. Sci. Eng.* **2017**, *3*, 153.
[29] M. C. Garnett, P. Kallinteri, *Occup. Med.* **2006**, *56*, 307.
[30] N. A. Bakh, A. B. Cortinas, M. A. Weiss, R. S. Langer, D. G. Anderson, Z. Gu, S. Dutta, M. S. Strano, *Nat. Chem.* **2017**, *9*, 937.
[31] S. N. Goyal, N. M. Reddy, K. R. Patil, K. T. Nakhate, S. Ojha, C. R. Patil, Y. O. Agrawal, *Chem.-Biol. Interact.* **2016**, *244*, 49.
[32] R. Xu, D. W. Greening, M. Chen, A. Rai, H. Ji, N. Takahashi, R. J. Simpson, *Proteomics* **2019**, *19*, 1700453.
[33] H. Yu, J. S. Palazzolo, J. Zhou, Y. Hu, B. Niego, S. Pan, Y. Ju, T.-Y. Wang, Z. Lin, C. E. Hagemeyer, F. Caruso, *ACS Appl. Mater. Interfaces* **2022**, *14*, 3740.